

Conceptual Design of a Satellite for GPS Attitude Based
Measurement of Thermospheric Winds

by

Christopher Lee Schierer
B. S. Mechanical Engineering May 1995
Rensselaer Polytechnic Institute

A Thesis submitted to

The Faculty of

The School of Engineering and Applied Science
of The George Washington University in partial satisfaction
of the degree of Master of Science

July 21, 1997

Thesis directed by

Dr. Robert H. Tolson



Abstract

Science measurements of the upper atmosphere are limited by the ability of spacecraft to obtain measurements of the sparse gasses. Using optical techniques limits the spatial resolution of the data, and may limit observations to solar day only. Complex sensing systems also require highly accurate pointing and attitude stability. A mechanical method may provide the answer to obtaining thermospheric wind measurements that have exceptional spatial and velocity resolutions. In addition, attitude stability can be achieved through passive means for simplicity of design.

The Global Positioning System (GPS) has become a tool well beyond its original design. One such expansion is the use of GPS carrier phase for attitude determination. By finding the phase difference between multiple antennae, a three dimensional attitude and position fix can be made. With increasing distance between antennae, more detailed attitude estimates can be made.

This study investigates the conceptual design of a satellite that will obtain wind measurements with accuracies that meet or exceed those available through conventional techniques. The spacecraft will be passively stabilized using gravity gradient and aerodynamic techniques. Science data will be obtained directly from the spacecraft attitude through the use of a Global Positioning System (GPS) carrier phase attitude system. The concept feasibility will be examined relating to technology limitations and areas requiring further investigation.

Acknowledgments

I would like to thank my thesis advisor, Dr. Tolson for the opportunity to work on this project. It was an exciting and challenging opportunity to design a novel new spacecraft concept. For all his support and suggestions throughout this thesis, again, I thank him. I also appreciate the time and effort of Dr. Whitesides and Dr. Juang for serving on my thesis committee.

Thanks also to Dave Skillman who provided some insights into small spacecraft design. He was also able to provide me with contacts on many questions that lead to solutions found in this report. I especially appreciate his patience as he explained various approaches to some of the problems I faced.

Special appreciation goes to the crew of Dr. Jer-Nan Juang's Spacecraft Design Course. The issues they helped resolve for the in class project often shed new insight on problems I was facing in this design. To James, George, and Jeff in particular for listening *ad nauseum* about which approach I was using for my thesis. In addition, Suzy deserves special commendation for putting up with my office antics.

Most of all, I owe everything to Kristin, who was there with supportive words, and a compassionate ear those times when I had more than I could manage... this is all for you.

Table of Contents

ABSTRACT	II
ACKNOWLEDGMENTS	III
TABLE OF CONTENTS	IV
LIST OF FIGURES	VI
LIST OF TABLES	VII
LIST OF SYMBOLS	VIII
I. INTRODUCTION	1
II. BACKGROUND INFORMATION	4
II.1. Thermosphere Environment	4
II.2. Wind Measurement Techniques	6
II.3. Aerostabilization	9
III. DESIGN	12
III.1. Satellite Overview and Layout	12
III.2. Mission Goals as Design Drivers	15
IV. GPS ATTITUDE MEASUREMENT	20
IV.1. Explanation of GPS Phase Attitude Determination	20
IV.2. State of the Art for Space Based Systems	22
IV.3. Mission Technology Needs	24
V. POWER SYSTEM	26
V.1. Power System Options	26
V.2. Power System Specifications	28
V.3. Remaining Issues	32
VI. THERMAL CONTROL	35
VI.1. Basic Thermal Model	35
VI.2. Split Geometry	36
VI.3. Partially Deployed Geometry	38
VI.4. Remaining Issues	41
VII. ATTITUDE CONTROL & STABILITY	42
VII.1. Gravity Gradient	43
VII.2. Aerodynamics	44
VII.2.1. Large Inline Tail Configuration	45
VII.2.2. Tail End Plate Configuration	48
VII.3. Damping Methods	53

VII.3.1. Fluid Ring Dampers	53
VII.3.2. Magnetic Hysteresis Dampers	57
VII.3.3. Viscoelastic Damper	57
VII.3.4. Active Damping	59
VII.4. Solar Torque	60
VII.5. Remaining Attitude Control Issues	61
VIII. COMMUNICATIONS	63
VIII.1. Data Volume and Rate	63
VIII.2. Link Analysis	65
IX. OTHER SUBSYSTEMS	67
IX.1. Data Handling and Subsystem Control	67
IX.2. Deployment Systems and Structure	69
X. OVERALL FEASIBILITY & CONCLUSIONS	74
XI. REFERENCES	77
APPENDIX A: SPACECRAFT SUMMARY	81

List of Figures

Figure II.1: General Aerodynamic Torque _____	10
Figure III.1: Isometric View of Satellite Layout _____	12
Figure III.2: Front and Top Views of Satellite Layout _____	13
Figure III.3: Possible Spacecraft Configurations _____	17
Figure IV.1: GPS Phase Difference Measurement _____	21
Figure VI.1: Basic Thermal Model _____	35
Figure VI.2: Hot Orbit Arrangement: No Eclipse Occurs _____	37
Figure VI.3: Cold Orbit Arrangement: Maximum Eclipse Occurs _____	38
Figure VI.4: Half Deployed Configuration _____	39
Figure VII.1: End Plate Configuration _____	43
Figure VII.2: Inline Tail Configuration _____	45
Figure VII.3: Satellite Response for Tail Configuration _____	47
Figure VII.4: Relationship between α , γ , and θ _____	50
Figure VII.5: Lifetime Vs Average Wind Measurement Error _____	51
Figure VII.6: Tail End Plate System Response for a 3 Month Lifetime _____	52
Figure VII.7: Fluid Ring Damper _____	53
Figure VII.8: Large Ring ($R_R=0.45\text{m}$): Damping Torque Vs. Time _____	56
Figure VII.9: Small Ring ($R_R=0.20\text{m}$): Damping Torque Vs. Time _____	56
Figure VII.10: Model Of Viscoelastic Damper for Satellite Dynamics _____	58
Figure VII.11: System Response With Linear Viscoelastic Mechanism _____	59
Figure IX.1: Stowed and Deployed Configurations _____	69
Figure IX.2: Sample Cross Sections of Deployable Booms _____	72
Figure A.1: Spacecraft Dimensions and Summary _____	80

List of Tables

Table II.1: Orbit Related Parameters for Constant Atmospheric Density	5
Table IV.1: Phase Measurement vs. Baseline Length	25
Table V.1: Secondary Cell Energy Densities	27
Table V.2: Worst Case Power Needs	29
Table VIII.1: Communications Link Budget	65

List of Symbols

A	$[m^2]$	General Surface Area
A_{EFF}	$[m^2]$	Effective Solar Panel Area
A_{PLATE}	$[m^2]$	End Plate Area
A_{PROJ}	$[m^2]$	Projected Area
A_{TAIL}	$[m^2]$	Inline Tail Area
C	$[N\cdot m\cdot s]$	Satellite Equivalent Damping Coefficient
C_D		Coefficient of Drag
C_V	$[N\cdot m\cdot s]$	Viscoelastic Rotational Coefficient of Damping
E	$[Pa]$	Young's Modulus
E_{BAT}	$[W\cdot hr]$	Battery Energy
E_{REQ}	$[W\cdot hr]$	Required Eclipse Energy
E_{SOLAR}	$[W\cdot hr]$	Solar Panel Energy Generation per Orbit
F_{DRAG}	$[N]$	Aerodynamic Drag Force
F_{RING}	$[N]$	Force Acting on Damper Ring Wall
I	$[m^4]$	Area Moment of Inertia
I_0	$[kg\cdot m^2]$	Dumbbell Mass Moment of Inertia About Dumbbell Axis
I_{PLATE}	$[kg\cdot m^2]$	Tail Boom With End Plate Mass Moment of Inertia
I_{SUN}	$[W/m^2]$	Solar Radiation Constant at Earth Orbital Radius
I_T	$[kg\cdot m^2]$	Total Satellite Yaw Mass Moment of Inertia
I_{TAIL}	$[kg\cdot m^2]$	Inline Tail Mass Moment of Inertia
I_Z	$[kg\cdot m^2]$	Spacecraft Mass Moment of Inertia About Z-Axis
J_0		Bessel's Function of the First Kind, Order Zero
K	$[N\cdot m]$	Satellite Equivalent Spring Constant
K_V	$[N\cdot m]$	Viscoelastic Rotational Spring Constant

k		Arbitrary Integer
L	[m]	Length of Tail Boom
M_{RING}	[N-m]	Moment of the Damper Ring About the Ring Axis
P_{HRS}	[hr]	Orbital Period
R	[m]	Outer Radius of Damper Tube
R_{CP}	[m]	Distance from Center of Mass to Center of Pressure
R_{R}	[m]	Radius of Damper Ring
r	[m]	Radial Position from Center of Damper Tube
T_{PLATE}	[N-m]	Torque Created by the End Plate
T_{TAIL}	[N-m]	Torque Created by the Inline Tail
t	[s]	Time
U_0	[m/s]	Maximum Velocity Of Damper Tube Wall
u	[m/s]	Fluid Velocity
W	[m]	Width of Inline Tail (Z direction)
α	[radian]	Angle of Attack
β		Complex Coefficient
γ	[radian]	Relative Wind Angle From Orbital Plane (Yaw Direction)
ζ		Dimensionless Damping Ratio
θ	[radian]	Spacecraft Yaw Angle
θ_1	[radian]	Yaw Angle of Dumbbell from Orbital Plane
θ_2	[radian]	Yaw Angle of Tail from orbital Plane
θ_{N}	[radian]	Wind Angle from Surface Normal
θ_{R}	[radian]	Angle About Axis of Damper Ring
λ	[m]	Wavelength
μ	[kg/(m-s)]	Fluid Viscosity
μ_{S}		Solar Panel Efficiency

I. Introduction

Scientific interest in the dynamics of the atmosphere have led to multiple atmospheric computer models based on thermodynamic processes. Particular interest lies in the region of the atmosphere known as the thermosphere. This region is defined by increasing temperature with altitude due to solar ultraviolet heating. These models are dependent on empirical measurements of the temperature, composition, and velocity of the gases. This study will examine the use of an inexpensive satellite to measure the thermospheric winds at low Earth orbit (LEO).

To obtain scientific data which is an addition to current knowledge, several requirements must be met. First, the craft must be able to measure the winds for a useful period of time. Current models show that changes in solar heating due to seasonal variation create dramatic changes in global wind patterns. It will therefore be necessary to maintain orbit for at least one entire season. Second, the resolution of the wind measurement must be competitive with current measurement techniques. This requires a velocity resolution of 10 m/s. Finally, coverage of the entire globe is required for a complete model. The polar region, in particular, exhibits wind variations with changes in magnetic activity that are of special interest. For this reason a polar orbit is used to provide global coverage.

To remain inexpensive, a novel measurement technique is being investigated. Previously, the best wind resolution has been obtained by limb-scanning instruments such as the Wind Imaging Interferometer (WINDII) and the High Resolution Doppler Imager

(HRDI) on the Upper Atmospheric Research Satellite (UARS) [1]. These devices use optical techniques to detect the Doppler shift in the emissions of solar excited gasses. This approach requires expensive optical equipment. The objective of this study is to use a more simple physical measurement technique. If the spacecraft is built in a way that the changes in wind speed will alter its attitude, attitude determination will provide science data. This attitude determination will be performed by a commercially available Global Positioning System (GPS) receiver capable of detecting the carrier phase differences between multiple antennae.

To begin this study it is important to understand the characteristics of this orbital environment. A brief introduction to the thermosphere and its physical environment will be presented. A background on wind measurement techniques will also be provided. The aerodynamic forces on a LEO satellite will be discussed with emphasis on the requirements for aerostabilization.

Once a foundation has been established, the next chapter will give a satellite and mission synopsis. The satellite layout and characteristics will be introduced so that a familiarity is established for the remainder of the study. The mission goals and the use of these goals to make design choices will be presented.

Following the overall layout and mission goals, each subsystem will be examined in turn. Each chapter will describe the requirements, possible components, and remaining issues for the respective subsystem. The use of GPS as an attitude measurement device will be analyzed and required capabilities noted. The attitude resolution will be discussed and compared with actual experimentation. The electrical power system will be introduced and capabilities compared to component requirements. A thermal analysis will be

performed to show that passive measures will be sufficient for spacecraft survival. Several simplified thermal models are presented in the extreme cases and the final configuration identified.

Since it is the goal to use the attitude as a science measurement, a chapter on the passive attitude control system is included. The use of gravity gradient stabilization in pitch and roll is presented. Simulations of spacecraft yawing motion due to wind changes are shown for an optimal geometric configuration. A discussion of damping methods is included with an emphasis on their effectiveness at small angular rates.

The final chapter will present an overview of the remaining subsystems. The link analysis for the communications system will show that sufficient technology exists for the required data rates. Computer control, data handling and storage needs will also be addressed with an overview of required computer tasks. Deployment devices will be handled in the final section to show that mission needs can be satisfied.

Once the design has been discussed and examined at the subsystem level, the overall concept feasibility will be established. It is desirable that a sufficient confidence can be obtained to encourage further investigation into the construction of such a spacecraft. Any specific outstanding issues will be identified and targeted for further study.

II. Background Information

Before discussing the design decisions and details, it is necessary to establish some understanding of the LEO environment. It is also important to discuss processes acting in this environment that will most affect the success of this mission. First, there will be an explanation of the upper atmospheric environment with emphasis on the region around 300 km of altitude. This region is known as the thermosphere.

II.1. Thermosphere Environment

The thermosphere is an atmospheric region defined by increasing temperature with altitude due to solar ultraviolet heating. This region exists above ~90 km and extends to ~600 km. The lowest extreme is characterized by a rapid increase in atmospheric temperature with altitude. At the upper boundary of this region, the temperature approaches a limiting value, the exospheric temperature. The exospheric temperature varies from ~600 to 1200 K depending on solar activity [2]. The amount of solar activity and the corresponding change in temperature also affects the atmospheric density.

The 1976 Standard Atmosphere [3] table states that the mean density at 300 km altitude is approximately $1.916 \times 10^{-11} \text{ kg/m}^3$. However, solar variation can cause an order of magnitude change in the density at this altitude. This design will only consider the case where the atmospheric density at 300 km is this standard value. This value directly affects lifetime estimations and attitude dynamic response. Recognize that as the satellite orbit decays the atmospheric density will increase. According to the MSIS-86 model results plotted in *Spacecraft Mission Analysis and Design* [2], this density represents a typical value for solar minimum (F10.7=75). The F10.7 index is a measure of the 10.7 cm radio

flux measured in units of 10^{-22} W/(m²-Hz). The index is a proxy for solar activity and levels of atmospheric density. Note that analysis of the spacecraft at this particular density leads to a requirement to launch to an orbit which this average density. Since this is a solar minimum value, the necessary altitude will increase as solar activity increases. At a solar index F10.7 of 225, MSIS-86 predicts an altitude requirement of 420 km. This will affect the subsystem analysis by changing the orbital period, and the ground station viewing slightly. In actuality, a higher altitude leads to a shorter maximum eclipse, and an extended ground station viewing time. Table II.1 shows the change in various orbit related parameters due to an increase in orbital altitude from 300 to 420 km due to solar activity. All parameters are for a circular orbit.

Orbit Related Parameter	F10.7=75	F10.7=225
Altitude [km]	300	420
Orbital Velocity [km/s]	7.73	7.65
Orbital Period [min]	91	93
Max. Eclipse [min]	37	36
Ground Station View 5° Elevation [min]	6.5	8.3

Table II.1: Orbit Related Parameters for Constant Atmospheric Density at Different Solar Activities

Due to the lower air densities at orbital altitude, the gas particles become further separated, and collisions between them become less frequent. The mean distance a particle travels between collisions is known as the mean free path. At 300 km altitude, the mean free path of the gas particles is very large relative to the dimensions of satellites. When the mean free path is much larger than the dimensions of an object in the flow, that object is considered to be in free-molecular flow.

In the free-molecular flow regime, a particle that collides with an obstruction (such as a spacecraft) is unlikely to encounter another particle within the dimensions of the obstruction. Generally, no collisions will occur between incoming particles and outgoing ones. Therefore, the downstream portions of a spacecraft can be considered shadowed by components upstream. For this study, the primary interest in the flow is in the calculation of drag coefficients. The calculation of this coefficient is based on careful observation of satellites in low Earth orbit and to a lesser extent ground based experimentation. For most satellite configurations Moe [4] states a value of 2.2. This coefficient value will lead to sufficient accuracy for this study.

II.2. Wind Measurement Techniques

Since the atmosphere varies with altitude, wind measurement techniques also vary. At the Earth's surface, meteorological stations use weather vanes and anemometers to measure local dynamics. They are inexpensive due to their mechanical simplicity, yet provide accurate real-time readings.

Ground based remote sensing stations use several techniques to develop wind speed data. Radar stations can track the position of airborne particles such as rain or snow over time to develop wind measurements. Doppler radar is also used to detect the relative velocity of airborne particles with respect to the ground station. This mapping of velocities may lead to storm warnings and is detailed enough to detect the rotary motion of tornadoes. Radar is also used to detect the motion of meteoritic ablation particles in the middle regions of the atmosphere [1]. The drawback of ground stations is their fixed position. Each station is limited to line of sight measurements. Combining the data from a network of

stations can provide wide area coverage. Where it is not practical to locate a sensor, data is unavailable.

Aircraft can also carry wind measuring instruments. Pressure sensors are used as altimeters and airspeed indicators. In addition, gas samples can be taken for composition analysis. When combined with the position and ground speed of the aircraft, a wind speed and direction are obtained. At altitudes inaccessible to winged aircraft wind patterns are monitored by weather balloons and sounding rockets. These craft are able to measure gas concentrations, barometric pressures, wind speed and many other parameters along the trajectory of their ascent and descent.

Satellite techniques offer the opportunity to measure global wind patterns remotely. Meteorological satellites obtain wide field of view images of water vapor motion in the atmosphere. These are able to give measurable results in the troposphere. At altitudes above ~20 km these satellites become less effective due to the low concentrations of water. Two sensors flown aboard UARS were designed to observe and record the wind velocity in the altitudes from 50 to 300 km. HRDI observes Doppler shifts in the O₂ emission lines. This provides daytime observations from 50 to 115 km in altitude. At night, a narrow O₂ emission layer is observed near 94 km limiting measurements to this altitude. WINDII detects photochemical airglow features in the 80 to 300 km region both day and night. Although the two sensors use different optical measurement techniques, they obtain wind vectors using Doppler shift. Two observations of each location are made from nearly orthogonal viewing directions. HRDI uses a fully gimbaled telescope, while WINDII uses two fixed telescopes at 45° and 135° to the satellite trajectory. Since each device is looking through a volume of the atmosphere, the images have limited spatial resolution. A specific weighted average is used to obtain altitude information. UARS is in a 57° inclination

circular orbit at 585 km altitude. Combined with the sideward imaging direction of the instruments, this orbit allows imaging of only the portion of the Earth between $\pm 74^\circ$ latitude [5,6]. Higher latitudes which contain the highest wind speeds and polar vortices are not viewable. Despite the limited spatial resolution and lack of polar measurements, the sensors on UARS represent the current state of the art for sensing in the atmospheric region above ~ 50 km.

Using data from many different sources, multiple atmospheric wind and composition models have been constructed. A comparison of several models and the UARS sensor products is available in Fleming et. al. 1996 [7]. Data for the poles is particularly desirable due to the effects of charged particles in this region during solar storms. It is the intent of this study to design an inexpensive satellite that can measure wind speeds with comparable or better spatial, temporal, and speed resolutions than currently available. Measurements of wind speed at orbital altitudes and with global coverage are also required.

The UARS sensors were able to detect a velocity within $\pm 5-10$ m/s, but due to the limb scanning technique spatial resolution is limited to 500 km. Altitude resolution is more precise at ± 3 km. For this study, the satellite location in three dimensions will be known within the accuracy of the GPS (± 0.1 km) which will correspond directly to the measurement location. The target wind speed resolution is $\pm 5-10$ m/s as achieved by the UARS instruments. The wind measurements will be limited by the attitude response of the satellite and the attitude resolution of the GPS device. The attitude response will be a function of the aerodynamics of the spacecraft. Attitude control through aerodynamic design is known as aerostabilization.

II.3. Aerostabilization

In conventional satellite design, the torques and forces created by atmospheric drag are considered disturbances. Using these torques to your advantage allows a passive control system to be constructed. Passive systems are generally lower in cost and higher in reliability due to a lack of complexity. The design of an aerostabilized satellite requires an understanding of the aerodynamic forces acting on the spacecraft.

For this discussion, the aerodynamic drag force is given by:

$$F_{DRAG} = \frac{1}{2} C_D A_{PROJ} \rho v^2$$

where C_D is the coefficient of drag for the body in free-molecular flow, A_{PROJ} is the projected surface area, ρ is the air density, and v is the wind stream velocity relative to the body. The force is proportional to the area projected perpendicular to the wind stream. To relate this area to the area of the satellite surfaces

$$F_{DRAG} = \frac{1}{2} C_D A \cos \theta_N \rho v^2$$

is obtained, where θ_N is the wind incident angle from the surface normal and A is the actual area of the body. Note that each portion of a spacecraft may have a different surface normal, the total drag would be the summation of each contribution. For most bodies, a standard value of 2.2 is used [4]. This is accurate for simple solids such as plates, spheres and cylinders.

In free molecular flow, the lift contribution is negligible relative to the drag force so it will be ignored for this analysis. The drag force acting on the spacecraft is considered to be concentrated at one point, the center of pressure. This center of pressure (CP) is located

at the centroid of the projected frontal area. In general, the CP will not coincide with the center of mass; the vector from the center of mass to the CP is shown in Figure II.1. Since there is a corrective torque generated by the drag acting at this distance, the spacecraft will align with the flow direction. Note that without the presence of damping an oscillating system is created.

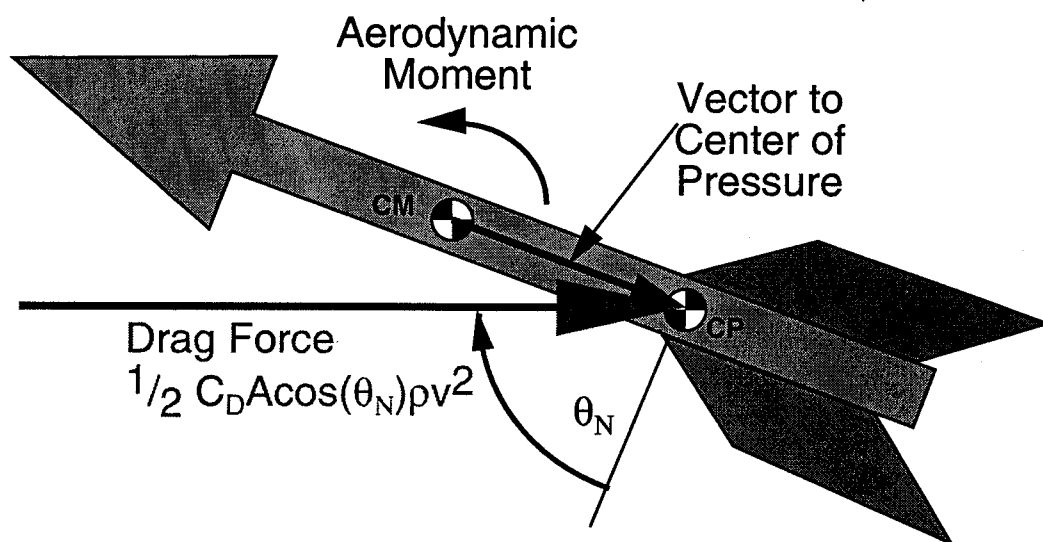


Figure II.1: General Aerodynamic Torque

For LEO applications, aerodynamic effects have traditionally been examined as disturbances to pointing or data collection. With the increased drive for smaller spacecraft, designers are looking to use passive methods of attitude control. One such experiment [8] launched from STS-77, is called PAMS (Passive Aerodynamically-Stabilized Magnetically-Damped Satellite). Developed at NASA's Goddard Space Flight Center, this unit is cylindrical in shape and contains magnetic hysteresis dampers. The center of mass is not geometrically centered so that a drag torque is created. With spherical inertial properties, the gravity gradient torques are removed, leaving the aerodynamic effect in control. Despite being launched with a higher than planned initial tumble, the craft was able to come

to a stable orientation in less than three days. This shows that aerodynamic torques can be used in a beneficial way. At this point, this discussion will continue with an overview of the concept as a whole, with some explanation of primary feasibility concerns.

III. Design

The design of any spacecraft is controlled by the intended mission. In the case of a conceptual study, it is important to establish which design parameters are fixed by mission constraints and which are feasibility drivers. In the case of this concept, a general design approach was established from the mission requirements. This is often true of risk mitigation flights which seek to validate a new technology or approach for future use. At this point in the conceptual design, it is important to establish the feasibility of the measurement technique as well as the spacecraft design.

III.1. Satellite Overview and Layout

The concept satellite is a low Earth orbit (LEO) platform for the measurement of thermospheric winds. It is gravity gradient and aerodynamically stabilized to provide fully passive attitude control. With a mass of 85kg and stowed dimensions of approximately 1x1x2 meters, it may be viable for secondary payload spaces in heavy launch platforms. When placed in a 300 km polar orbit, measurements can be made that cover the entire globe

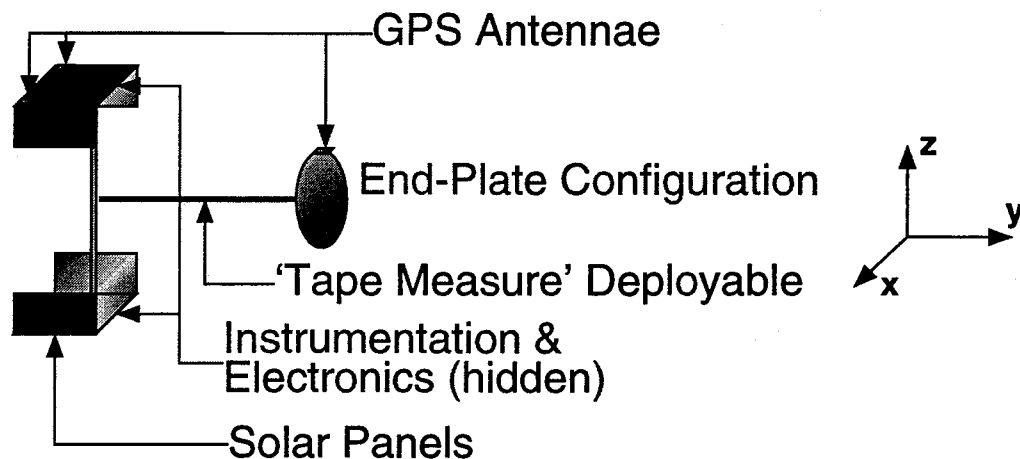


Figure III.1: Isometric View of Satellite Layout

as the Earth rotates. All science data will be retrieved directly from the GPS attitude system, and stored for daily downlink. The physical layout is specifically designed to minimize frontal area, while maximizing the wind torque about the yaw (Z) axis. A layout drawing of the spacecraft configuration is included as Figure III.1 and III.2. A system summary is also given in Appendix A.

The solar panels are arranged to provide at least 0.81 m^2 of surface area regardless of the orbital orientation with respect to the sun. Only 0.64 m^2 is necessary to meet power requirements, but to achieve a standard voltage of 28 Volts, the solar cells must be arranged in strings of at least 32 cells. Each string requires approximately 0.20 m^2 . The minimum solar exposure per orbit occurs when the sun lies in the orbital plane and this condition was used to size the system. This orbit also contains the peak solar power wattage when the spacecraft nears local solar noon. The power bus is sized to handle this maximum 8.0 Ampere, 224 Watt peak. During eclipse, power is provided by NiCd rechargeable cells at 28 Volts. Nominally the spacecraft requires 35 W-hrs per orbit of energy which is

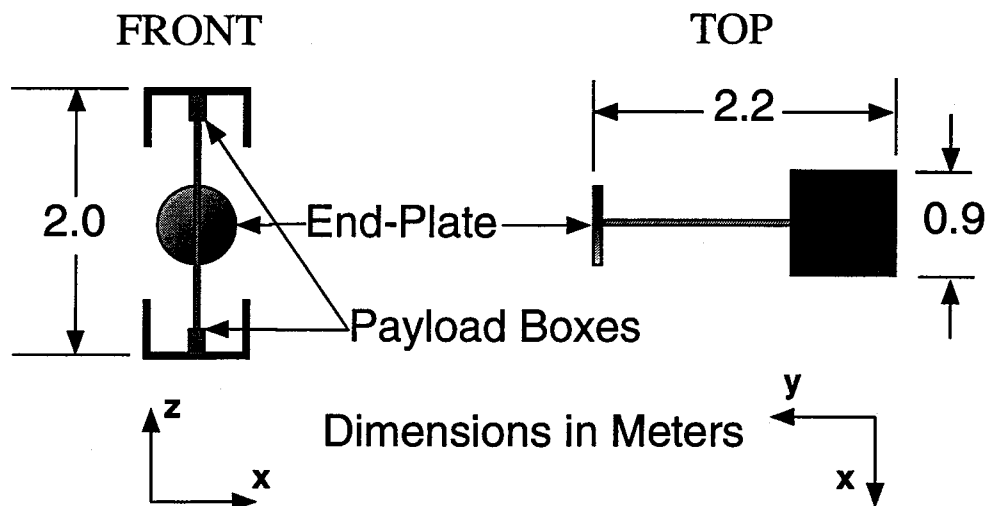


Figure III.2: Front and Top Views of Satellite Layout

provided with at least 50% margin due to the solar cell strings required for standard voltage.

The GPS attitude system will use antennas placed at the end of the tail and on the solar arrays. There will be redundant antennas on both the +Z and -Z sides of the satellite. Phase measurements will be made on-board, and attitude information stored in onboard memory. The choice of determination algorithms is beyond the scope of this study, but further information can be found in Cohen 1996 [9]. Some discussion on the theory of the system is included in Chapter IV. In the absence of significant multipath error, a phase determination within ± 1 mm can be obtained. A 1.5 meter baseline provided by the tail-boom will provide a theoretical attitude resolution of 0.038 degrees (0.67 mradians) in pitch and yaw. This would limit wind measurement resolution to 5 m/s. Roll determination would be limited to 0.064 degrees (1.1 mradians) by the 0.9 meter baseline across the solar array.

To extend the satellite lifetime, it was important to minimize the drag forces. The payload section of the spacecraft can be designed to do this at equilibrium by aligning the maximum dimensions with the wind direction (y-axis). The plate is not aligned in this manner, but instead provides maximum area to the wind stream. For the plate, the changes in drag due to small variations about equilibrium will be small. The tail plate will be 0.36 m² in area and use a 1.5 m moment arm to optimize the relationship between tracking and lifetime.

Two options prevent solar pressure from having a detrimental influence on the spacecraft. The first involves the use of a reflective plate, the maximum deflection caused by solar pressure would be 7.7 mradians. This would require modeling solar torque based

on current solar position relative to the spacecraft and an understanding of the optical properties of the spacecraft surfaces. Alternately, a transparent film may be used for the plate. A 90% transparent film would lead to a maximum deflection of 0.38 mradians due to solar effects. This deflection would be smaller than the wind measurement resolution of the spacecraft and would not require modeling of the solar torque. Either option is within current technology and would primarily affect the choice of plate material.

The plate would be supported by a “carpenter’s tape” type deployment system. A single tape would be used to deploy an oxygen resistant film or foil plate at the necessary length. The GPS antenna wires for the plate mounted antennae will pass along this tape and would be deployed with it. A telescoping tube may also be a viable deployment option.

Communications will be handled through a small commercial transmitter/receiver pair in the low S-band range. Data will be stored onboard, until the satellite passes within view of a designated ground station. A 12 dB link margin has been established using a 1 Watt output radio frequency transmitter. Data will be sent on command by the ground station to ensure that sufficient communication lock has been established. The specifications of a commercially available 1 Watt device are used throughout this study as a representative example.

III.2. Mission Goals as Design Drivers

For an aerodynamic wind measuring craft, there were several issues to be addressed. It is the intent to reduce cost by using passive attitude control, a physical wind sensing method, and a GPS attitude measurement system. Some of the major issues that

were first identified were the effect of gravity gradients on long thin spacecraft, the limits of the GPS system to return sufficient angular information, and sufficient lifetime for scientific usefulness.

The resolution of a GPS attitude determination is dependent on the baseline length between multiple antennae. A more detailed explanation of the attitude determination technique follows in Chapter IV. It is also clear that an increase in length, permits an increased moment arm for the aerodynamic drag force as well as increased rotational inertia. This increased length also leads to a larger gravity gradient torque. The craft must be free to move relative to the changing wind direction. For a polar orbit, the zonal winds are of interest, and the motion to be measured should occur in the yawing direction.

Several satellite configurations were identified and are shown in Figure III.3. Each of these configurations rely on aerodynamic torques to keep the craft pointed into the wind. In the arrow and string designs, the aerodynamics control the yaw as well as the pitch direction. The arrow is the direct extension of the classical weathervane. Recall that gravity gradient torques tend to align the minimum moment of inertia with the nadir direction. In these designs, the aerodynamic torque resists pitching due to the gravity gradient effect. The spacecraft will align in an equilibrium position where the aerodynamic pitching torque cancels the gravity gradient. Since the craft will not be aligned with the wind vector, the frontal area will not be minimized which leads to a shortened lifetime. Since the aerodynamic torque is proportional to length and gravity gradient moment increases with the square of length, the desired alignment is difficult to create with these approaches. The dumbbell concepts, however, are not limited by gravity gradient torques.

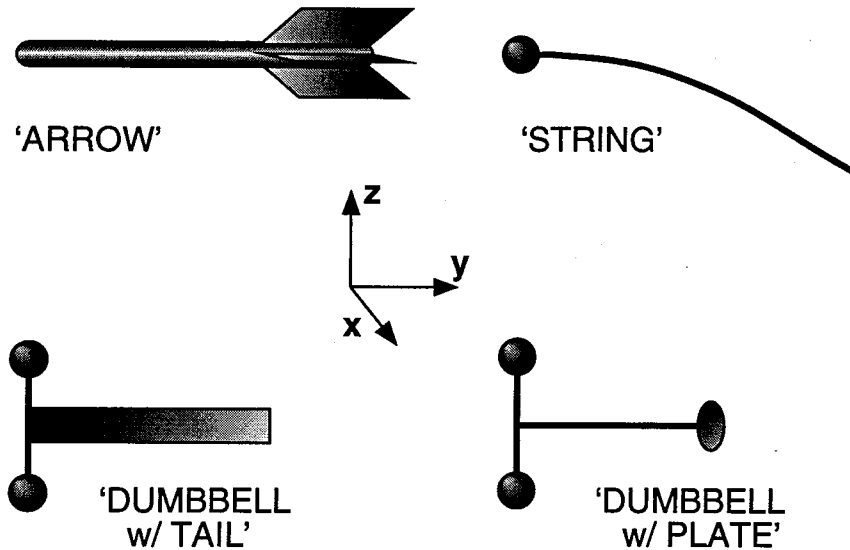


Figure III.3: Possible Spacecraft Configurations

For the two dumbbell approaches shown above, the satellite is constructed to take advantage of gravity gradient stabilization. By designing the minimum moment of inertia to lie in a desirable direction, the craft can be caused to orient in an advantageous way. In these configurations, the pitch and roll directions are controlled by the gravity gradient torques, and the wind affects only the yawing motion. Note that the length of the tail is limited by the requirement that the minimum moment of inertia be in the Z direction.

Differences between the inline tail and the end-plate configurations will be discussed throughout the paper. The primary differences occur in the aerodynamic response. For a fixed area the drag force varies with the cosine of the angle between the surface normal and the relative wind direction. As shown in Figure II.1, the torque is given by the force and the normal component of the CP vector relative to the wind flow. This moment arm also varies with the cosine. The CP vector itself would be the same direction in either craft. The plate, however, is perpendicular to the active surface in the inline tail arrangement. The following equations demonstrate the difference between the two configurations.

$$T_{TAIL} = \frac{1}{2} C_D \rho v^2 A_{TAIL} R_{CP} \cos^2 \theta_N$$

$$T_{PLATE} = \frac{1}{2} C_D \rho v^2 A_{PLATE} R_{CP} \cos \theta_N \cos(\theta_N - 90^\circ)$$

When θ_N approaches 90° , the torque goes to zero and either configuration will approach equilibrium. For a small perturbation, α , around equilibrium the equations become

$$T_{TAIL} = \frac{1}{2} C_D \rho v^2 A_{TAIL} R_{CP} \alpha^2$$

$$T_{PLATE} = \frac{1}{2} C_D \rho v^2 A_{PLATE} R_{CP} \alpha$$

where $\alpha = \theta_N - 90^\circ$

Due to the squared term in the tail torque equation, very small variations lead to negligible response, while the plate system acts proportionally. For a 10 m/s wind, the incident angle is on the order of 1 mradian. The tail response would then be on the order of 10^{-6} versus the plate on the order of 10^{-3} . These small responses correspond to science data which would be lost to the inline tail configuration. The plate torque equation above leads to the dynamics of a harmonic oscillator for small angular displacements. Attitude simulations of both cases are included in Chapter VII. The inline tail design is eliminated due to insufficient wind tracking response relative to the end plate configuration.

The disadvantage of the end plate system, is the increased drag force acting to shorten the spacecraft lifetime. With the inline tail, the frontal area is minimized in equilibrium, while the end plate area is maximized. Despite the shortened lifetime relative to the inline tail approach, the end plate will lead to improved science measurements. An examination of the relationship between lifetime and wind measurement is included in Chapter VII.

Each subsystem will be discussed throughout the remainder of this report. The system design will be described in detail, and where appropriate, a brief description of some other alternatives will be included for comparison. Each section will conclude by identifying the remaining issues which will need to be resolved in the next design phase.

IV. GPS Attitude Measurement

One of the satellite design goals was to incorporate a GPS unit for attitude sensing. Since the spacecraft attitude is directly related to the science data being measured, it is important to understand the attitude determination process. This process is described briefly along with an examination of the available GPS attitude sensing capabilities. A discussion of the mission requirements for the attitude sensor is also included.

IV.1. Explanation of GPS Phase Attitude Determination

The Global Positioning System (GPS) is being used increasingly for navigational purposes in ground based applications. The system consists of 24 satellites which broadcast pseudo-random time and ephemeris codes continuously. By comparing the time delay between 4 GPS satellite timing signals, a location can be determined within 20 meters in three dimensions. More recently, commercial attitude determination devices have been constructed. These systems use measurements of the carrier wave phase difference between multiple antennae to determine angular orientation and improve relative position accuracy.

The public GPS transmissions are broadcast at 1.58 GHz. At this frequency the wavelength is 19 cm. This leads to 0.5 mm per degree of phase. Using multiple antennas and precise phase measurements the orientation of the antennas in space can be determined. A two-dimensional example is shown in Figure IV.1. If only the phase measurement is known ($\Delta\phi$), an ambiguity can arise due to an indeterminate number of integral wavelengths between antennas ($k\lambda$). There are multiple approaches to this problem including placing an extra antenna within one wavelength of a primary antenna to get a

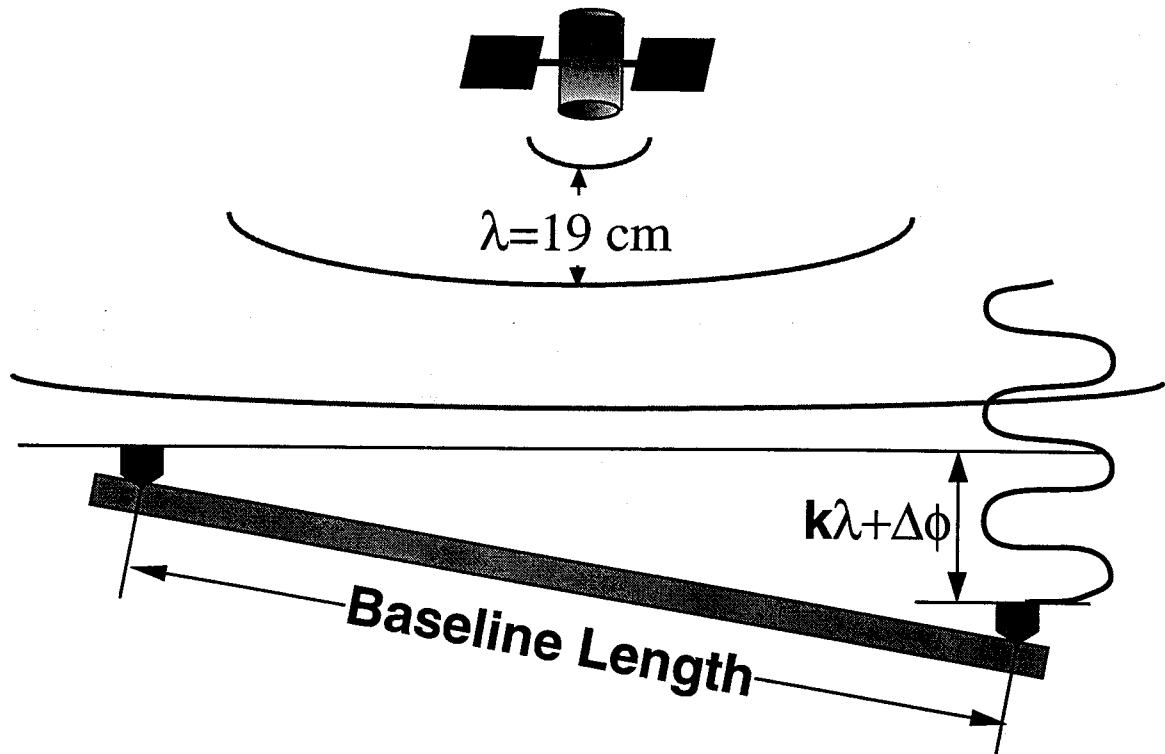


Figure IV.1: GPS Phase Difference Measurement

rough determination without ambiguity. Numerous mathematical approaches including integer searches and state estimation have been proposed to resolve this issue. A more detailed discussion of this concern can be found in Cohen, 1996 [9]. In this application once the spacecraft has reached equilibrium, the phase measurements will always be less than one wavelength. For most of the mission phase ambiguity will not be a concern.

For a three dimensional attitude fix it is likely that four satellites will need to be tracked at once. On the ground, GPS satellite 'tracking' is performed by merely predicting which satellites will be overhead at any given time, and scanning the frequency band for that particular signal. In space, the viewing becomes more complex since the receiver's velocity relative to the satellite has been greatly increased. The GPS satellites are in orbit at an altitude of approximately 18,000 km; this gives each craft a velocity of 4 km/s. A LEO craft at 300 km altitude travels nearly 8 km/s. The combined speed of 12 km/s causes

enough Doppler shift to prevent reception and lock for ordinary ground receivers. Special receivers have been designed that predict the Doppler shifts from a set of preprogrammed orbital parameters. If lock can be established then these parameters can be updated from the regular GPS transmissions and more accurate fixes established. There is considerable development in orbital GPS detection currently underway. The next section briefly describes the current state of the art in satellite capable systems.

IV.2. State of the Art for Space Based Systems

Space flight GPS systems have developed from aircraft systems with modifications to account for the lockup and tracking difficulties. The International Space Station will use GPS to determine attitude, position, and time. A recent system was flown on STS-77 as a shuttle cargo bay experiment. The GPS Attitude and Navigation Experiment (GANE) [10] was flown as a risk-mitigation flight for the International Space Station. GANE used a commercially available receiver combined with station specific components. Using a nearly rigid platform mounted on a Hitchhiker payload bridge in the cargo bay of the shuttle, the experiment was able to obtain real time attitude information. After post flight analysis, the experimenters have obtained solutions with ± 3.5 mradians (0.2°) attitude precision. Since the baseline length is 3.5 meters this would require a phase measurement of 1.2 cm. It should be understood that the primary error contribution for this experiment is multipath signal noise.

Multipath is a phenomenon that is caused by the incoming GPS transmission reflecting off surfaces near the antenna. The reflected transmission will travel a greater distance than the direct transmission leading to a phase difference. The effect appears as signal noise in the phase determination. In the case of the GANE flight, the antennae were

surface mounted on a large plate in the payload bay of the space shuttle. The space shuttle represents a large reflective surface relative to the area of the antenna array. In the case of a long deployed boom, there is little area for multipath in the view of the antenna. If the boom is of the same dimension as the remainder of the spacecraft, multipath will need to be carefully examined. Since it depends on spacecraft configuration, an exact estimate of this error source is not available, but certainly it would be significantly lower than the errors in GANE. In Cohen 1996 [9], “empirical tests have shown that for complex reflective surfaces, such as spacecraft, a conservative value for carrier phase error caused by multipath is approximately 5mm rms.” If this is true in the case of GANE, approximately half of the determination error is due to multipath.

In Osborne 1996 [11], phase differences are plotted for a ground based GPS attitude experiment. An optimistic approximation can be made by examining the noise in these phase measurements. Analyzing one such plot [11, Figure 7], a high frequency random noise is observable along with a lower frequency oscillation. This low frequency oscillation occurred primarily when the viewed satellite approached the horizon. Multipath causes such disturbances as the GPS signal reflects off the ground or other nearby objects. The higher frequency noise bounds the ideal case when multipath has no effect. Note that some portion of this noise is due to atmospheric effects which would not be present in space. The high frequency noise in this experiment is approximately 0.01 cycles RMS amplitude. This corresponds to a phase measurement of 1.9 mm, an attitude measurement within 1.3 mradians (0.076°), or a wind determination within 10 m/s for a 1.5 m baseline.

The Osborne results are based on a ground based experiment with a higher sampling rate than would be required for this mission. The spacecraft device would be free of the atmospheric interference present in the ground unit. In addition, averaging can be

used to reduce the noise further. If averaging could be used in combination with the lack of interference, to reduce the noise by 50%, a 1 mm phase measurement would be possible. This probably represents the lower limit for attitude determination at this time. At 1.5 meters, this corresponds to an attitude resolution of 0.67 mradians (0.038°), or a 5 m/s wind resolution. A 1 mm phase determination will be used to determine the optimal boom length and throughout the remainder of this analysis. The optimization process will be further explained in Chapter VII. Since the GPS unit will also provide accurate position information (within 100 meters), the wind data will have an instantaneous location reference that is several orders of magnitude better than limb scanning techniques.

IV.3. Mission Technology Needs

Since this GPS technology is still being developed, it would be useful to identify the particular needs of this mission, in the hopes that a future advancement might better satisfy the requirements. In this satellite, there is an ambiguity in the final orientation of the spacecraft. Although the attitude stability will be discussed in Chapter VII, it is sufficient to say that the satellite may orient in one of two ways, which are 180° of roll apart. Since it is unknown which side of the craft will stabilize in the local vertical direction, it is necessary to have complete redundancy of the GPS antennas. It will be necessary to incorporate this redundancy into the GPS system. This could be implemented through software or perhaps by electronically selecting antennas with the highest signal to noise ratios.

In addition to overcoming the added complexity of lockup in space, it would be beneficial if the system did not require initial information. Some systems require approximate locations to properly predict GPS satellite locations. Since this mission would not be the primary launch payload, it is likely that some injection uncertainty will be

present. If the location estimate was off by more than what the receiver can compensate for, a lock may not be established. If the system were capable of establishing a lock without initial information, this could be avoided.

Of course, it is necessary that the system remove integer wavelength ambiguity, and make phase measurements for attitude determination. To remain competitive with contemporary measurement techniques, phase measurements will need to have uncertainties similar to those discussed previously. This will provide relative wind speed measurements within 5 m/s for a 1.5 m boom. If this can be achieved, then the science data will be a useful addition to current atmospheric knowledge. Table IV.1 shows the relationship between phase measurement and baseline length for a ± 5 m/s wind determination.

Baseline Length	[meter]	0.5	1.0	1.5	3.0	5.0
Phase	[radian]	0.01	0.02	0.03	0.10	0.17
Measurement	[mm]	0.32	0.65	0.97	1.9	3.2

Table IV.1: Phase Measurement vs. Baseline Length

As expected, the phase measurement must improve as the baseline decreases for any given wind resolution. It is advantageous to obtain the best possible phase measurements because the corresponding science data would improve. The costs for the deployable boom structure would also decrease if it could be shortened. As will be shown in Chapter VII, a shorter boom also leads to improved tracking performance. With an understanding of how science data will be obtained, examinations of the other spacecraft subsystems follow. The power, thermal control, and passive attitude control system will each be addressed in detail. Communications, computer processor needs and deployment mechanisms will also be discussed.

V. Power System

Electrical power will be provided by fixed solar arrays. These arrays will generate a peak power of 224 Watts, with a minimum energy per orbit of 33 Watt-hours. During eclipse, power is provided by rechargeable Nickel-Cadmium cells with 1.5 Amp-hours of capacity at 40% depth of discharge. The charging system will undergo no more than 5000 cycles in a year, keeping in mind that there will be no eclipse for portions of the year.

V.1. Power System Options

There are three methods for primary power generation in space. They are chemical primary (non-rechargeable) batteries, radioisotope generators, and solar power.

Primary batteries are used in very short duration missions and would not support the three month target of this mission. The approximate per orbit energy need is 35 W-hrs; for ~480 orbits per month, 50 kW-hrs would be required. For a state-of-the-art battery energy density of 300 W-hrs/kg, a 170 kg battery would be required [12].

Radioisotope Thermoelectric Generators (RTG) are one type of radioisotope based power system. They are capable of generating up to 500 W continuously over a long mission. Typical uses include deep space probes, and military applications. They carry the added radioactive hazard that is politically unacceptable for a three month LEO mission.

The most common technology used in missions of this type is solar power. Using standard amorphous silicon solar arrays, efficiencies of 12% can be obtained. Efficiencies up to 25% have been demonstrated in laboratories using Gallium Arsenide (GaAs) solar

cells. Power generation is limited only by mission parameters such as altitude and inclination, and acceptable array size. For the low cost purposes of this mission, the array should be limited to body mounted, or fixed deployed arrays. Sun tracking arrays will not be possible due to the lack of active attitude control. Solar power requires the use of an alternate energy source during eclipse. Generally secondary (rechargeable) batteries are used to supply energy during dark portions of the orbit.

Table V.1 shows values representing state of the art [12,13,14] capability for secondary cells, although at this time only the first four types are readily available for space applications. Advanced technologies in this field are not examined due to limited power needs, and the cost constraints of new techniques.

Cell Type	Specific Energy (W-hr/kg)	Energy Density (W-hr/l)
Nickel-Cadmium (NiCd)	36	70
Nickel-Hydrogen (NiH ₂)	52	60
Nickel-Metal Hydride (NiMH)	60	145
Lithium Ion (Li-Ion)	100	240
Silver Zinc (AgZn)	90	
Sodium Sulfur (NaS)	200	140
Lithium Polymer	20	40

Table V.1: Secondary Cell Energy Densities

At this time, Li-Ion cells remain expensive and have outstanding safety concerns. If punctured or damaged, Li-Ion batteries have been known to ignite or even explode. NiMH provides the smallest and lightest package of the remaining technologies, but has limited cycle life. Some experiments have shown 1-3 year LEO lifetimes with very low depth of discharge (D.O.D.), but generally they are rated at a maximum of 500 cycles.

NiH₂ requires a pressure vessel for the containment of hydrogen gas. This tends to make them bulky, and difficult to construct for cell capacities similar to those needed for this experiment. NiCd remains the most reasonable option for this mission and is advantageously inexpensive.

Despite having poor specific energy even in advanced models, nickel-cadmium cells remain an effective choice. With high cycle life (>50,000 cycles for 30% D.O.D. at 0 °C [15]) and a long space heritage, they are common in LEO satellites. In the case of this mission, the additional mass of a NiCd cell over NiMH is not a concern, since additional mass will be necessary to extend the lifetime. Unfortunately, very small capacity cells are not currently available for space applications. The smallest commercially available, space qualified NiCd cells are around 4.5 Amp-hours. To obtain sufficient bus voltage, many cells would need to be linked in series to form one 28 Volt battery. Note the distinction between cell and battery. In this study cell will refer to a single 1.2 Volt NiCd electrochemical unit, while battery will refer to one or more cells united to provide additional current or voltage.

V.2. Power System Specifications

To determine solar panel size, the power drain of the component systems was analyzed. Each device has specific needs and duty cycle requirements during the life of the craft. To assure sufficient power generation, the maximum needs must be compared to the minimum available solar exposure. Table V.2 contains an analysis of the electronic systems and the corresponding power requirement for the satellite. This table represents the highest power use situation, i.e. when the daily data transmission must occur during eclipse. The operation of the transmitter represents the peak power usage for the

spacecraft. The longest possible eclipse was used to size the power system components since this would be the most demanding situation. All other orbits would have shorter eclipses, providing addition power margin for the satellite.

Transmit During Eclipse					
Eclipse:	<i>Current (A)</i>	<i>Power (W)</i>	<i>Max. Minutes</i>	<i>Max. Hours</i>	<i>Energy (W*hr)</i>
Transmitter	0.6	16.8	7	0.12	1.96
Receiver	0.1	3.1	37	0.62	1.91
G.P.S.	0.3	7.5	37	0.62	4.63
Power Losses	0.2	4.5	0	0.00	0.00
System Processor	0.3	7.0	37	0.62	4.32
Peak/Total	1.4	38.9			12.8
Orbital Period	93	minutes			
Maximum Eclipse	37	minutes			
Bus Voltage	28.0	Volts			
Daylight	<i>Current (A)</i>	<i>Power (W)</i>	<i>Max. Minutes</i>	<i>Max. Hours</i>	<i>Energy (W*hr)</i>
Transmitter	0.6	16.8	0	0.00	0.00
Receiver	0.1	3.1	56	0.93	2.89
G.P.S.	0.3	7.5	56	0.93	7.00
Power Losses	0.2	4.5	56	0.93	4.20
System Processor	0.3	7.0	56	0.93	6.53
Peak/Total	1.4	38.9			20.6
Eclipse Energy:	12.8	Watt*hrs			
Daylight Energy:	20.6	Watt*hrs			
Total Energy:	33.4	Watt*hrs			

Table V.2: Worst Case Power Needs

Since the only power source is the sun, the arrays must be sized so that the minimum exposure provides adequate energy. Since the attitude is not actively controlled, fixed arrays were chosen for this evaluation. A minimum area of 0.81 m² will be exposed to sunlight during the daylight portion of the orbit. The arrays will be oriented to present minimal surface area to the relative wind stream while maintaining the required solar exposure. Since the arrays are arranged on the top, bottom, and sides of the craft, the lowest power orbital arrangement is when the sun is in the orbital plane (Y-Z plane).

Relative to the spacecraft, the sun will rise in front (+Y), and pass over the top (+Z) of the craft, setting behind the tail (-Y). The only exposed panel will be the top one (+Z), and it will have an effective area that is proportional to the cosine of the angle between the sun and the panel normal. Over one pass, the average effective area is given by the following relationship:

$$A_{EFF} \approx \frac{\int_0^{\pi} A \cos(\psi) d\psi}{\pi} = A/2$$

where ψ is the angle of integration about half the satellite orbit. Note π radians in the denominator is the angular range of the integration. This establishes an average area across the entire pass.

To determine the total energy the average effective area must be multiplied by the solar constant, the efficiency, and the total exposure time. For silicon based panels, the efficiency is 10 to 12%. Higher efficiencies can be obtained with special care, and with other more expensive materials such as GaAs. Assuming that power is only obtained for one half of the orbit, the total exposure is half the period, or 46 minutes. This would represent slightly less than the minimum possible exposure for a conservative estimate.

$$\begin{aligned} I_{SUN} &= 1360 \text{ W/m}^2 \\ E_{SOLAR} &= \mu_s A_{EFF} I_{SUN} \frac{P_{HRS}}{2} \\ &= 0.10 * \frac{0.8}{2} * 1360 * \frac{1.5}{2} = 40 \text{ W * hrs} \end{aligned}$$

This minimum energy is more than sufficient to satisfy the worst case orbital pass. It should be noted, that only one orbit per day will involve a data transmission. Each of the remaining 15 orbits will result in 2 W-hrs of surplus energy, for a total of 30 W-hrs of

additional margin for the spacecraft. Once the cells are fully charged excess energy will be radiated from the solar arrays rather than converted to electricity.

The batteries can be sized by examining the needs of the same worst case orbit. The other major factor for battery design is cycle life. For most rechargeable cells, cycle life is inversely related to depth of discharge (DOD). DOD is defined as the percentage of the maximum obtainable energy that is used in any given discharge cycle. In the use of nickel cadmium (NiCd) cells, a DOD of 40% is recommended for a one year LEO lifetime at 25°C [15]. Although this is four times longer than the expected three month life, the operating temperature will be higher, limiting the battery effectiveness. With the mission life reduced to three months by the aerodynamic drag, a higher DOD is possible. Over extended cycle life, NiCd batteries may require conditioning. This is a process which consists of discharging the cells to nearly 100% DOD and recharging them fully. If conditioning does not occur, cells may develop 'memory' where the maximum available energy decreases. During periods where the eclipse is very short or non-existent, it is likely that this could be performed. Information regarding specific conditioning needs and cell life is particular to the cell manufacturer and beyond the scope of this report.

To size a rechargeable battery system, the amount of energy required for the eclipse portion of the orbit is divided by the depth of discharge to get the total capacity. In this case, Table V.2 gives the maximum required eclipse energy as 15.6 W-hrs. To allow 40% DOD, the required size is given by:

$$E_{BAT} = \frac{E_{REQ}}{DOD} = 15.6 / 40\% \approx 40 \text{ W * hrs}$$

Battery capacity (Amp-hrs) is obtained by dividing the required energy by the bus voltage (28 V) and rounding up to 1.5 Amp-hrs. Battery mass and volume can be approximated by

dividing the required energy by the energy density of the NiCd battery type. For a specific energy of 36 W-hr/kg the battery pack would have a mass of 1.1 kg. The volume of the unit would be 570 cm³ for the NiCd energy density of 0.07 W-hr/cm³. This volume will be packaged 6 x 8 x 12 cm to fit inside the payload box. Note that the battery was not sized for the energy surplus mentioned above, but this could be added if additional margin was deemed necessary.

At this time, the 1.5 A-hr cell is sufficient, so further calculations will be based on this quantity. In orbits where transmission does not occur, the DOD will be 33%. It is worth mentioning that the smallest space-qualified 'off-the-shelf' cells are 4.5 - 5 A-hrs by 1.2 Volts. Although obtaining a smaller capacity cell might require additional front end cost in design and construction, it may be worth considering due to the spatial constraints of the larger commercially available cells. A 28 Volt battery formed from these 4.5 A-hr cells would correspond to over 125 W-hrs of power, when only 40 W-hrs are required. Some possible approaches to this and other outstanding issues are discussed in the next section.

V.3. Remaining Issues

Some remaining considerations lie in the area of power management and charge control. Since the electronic 'user' components are sensitive to the input voltage, it will be necessary to regulate the bus voltage at a specific voltage. This can be achieved through various means, but generally with a 5-10% loss in power. It is also important to regulate power during the sunlit portion of the orbit since the incoming power will vary from zero to a peak of 120 Watts. During low power conditions it will be necessary to continue drawing from the batteries until sufficient solar power is obtained. During the peak power

conditions energy will be used to charge the battery packs and possibly perform battery conditioning.

One power management issue lies in the actual battery pack design. Each spacecraft component has a power need as well as a voltage requirement. If the battery pack is directly connected to the bus, it would need to have a potential of 28 Volts. However, NiCd cells have voltages from 1.2 to 1.5 V. To provide 1.5 A-hrs at 28 Volts, between 20 and 25 cells would be required in series. The alternative is to use several larger capacity cells, and use a voltage stepping device to increase voltage output. Since the minimum available cell is 4.5 A-hrs, the stepping option seems more promising. In this case, only 8 or 9 cells would be required to get the necessary total power output. However, this would provide only a 10 to 12 Volt battery before stepping. If voltage stepping is not a viable option, a custom battery pack may be required for a more efficient use of space. This custom 28 Volt battery would consist of 25 1.5 A-hr, 1.2 Volt NiCd cells in series.

It will be important to properly regulate the batteries. Excessive current can damage cells and cause a shortened lifetime. Charging control systems generally use a rapid charge until the cells approach capacity followed by a trickle charge to complete the energy transfer. Overcharging is prevented, and battery lifetime is maximized. It would be necessary to design the charge control system wiring and output to match the battery configuration chosen above. Although there are still some implementation issues in the power system, it is clear that the available technology is sufficient for this mission. It is possible that a custom designed battery and charge control device may be necessary, so the issues are in commercial availability rather than any limiting technology. The satellite has been designed conservatively to have enough power under the worst case conditions.

When the satellite is not transmitting during an orbit, or the sun lies outside the orbit plane, there will be as much as 75% more solar energy available. Also, eclipse lengths will generally be shorter than this worst case pass providing additional battery margin.

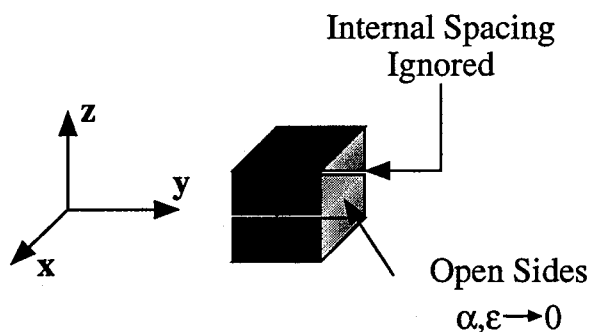
VI. Thermal Control

Many small satellites can perform passive thermal control through the use of insulation and thermal coatings. By properly balancing the solar absorptivity (α) and the infra-red emmissivity (ϵ) acceptable temperature ranges can be obtained throughout the craft. Unfortunately, for this satellite, most of the outer surface is covered with solar panels which have fixed thermal properties. With proper design, passive radiation should still be sufficient to maintain acceptable temperatures.

To properly analyze the thermal system, an iterative approach is used. Preliminary values are chosen from a geometrically simplified model of the spacecraft, and used to calculate conditions on a more detailed model. In this study, the process will be continued to a system level, where physical sections of the spacecraft will be treated as lumped components. The thermal effect of the tail section will be neglected in this analysis.

VI.1. Basic Thermal Model

For the first model, the vertical spacing between solar arrays will be ignored and an open ended box will be examined. Figure VI.1 shows the basic thermal model. It is assumed that sufficient conduction exists such that all surfaces are in static equilibrium and



therefore isothermal. The absorption and emission characteristics of four sides are controlled by the solar arrays ($\alpha=0.73$, $\epsilon=0.88$), while the two open sides will be modeled by low α and ϵ . The energy input to the system include direct solar,

Figure VI.1: Basic Thermal Model

Earth albedo, and Earth infra-red. Direct solar is the radiation that is output by the sun as a wide spectrum source at 1360 Watts/meter². Earth albedo is the effect of sunlight reflecting off the Earth with an approximate power flux of 400 W/m². Finally, the Earth emits infrared as a black body radiator at 298°K.

For a spacecraft at an altitude of 300km, the Earth subtends 45% of the sphere viewable by the spacecraft. The satellite will always have a face towards the Earth, while the sun facing array will vary throughout the year. In the worst case orbital orientation, a side of the satellite faces the sun throughout the orbit. The sunlight will be perpendicular to the Y-Z plane only at equinox. The top (+Z) faces deep space, and the bottom (-Z) faces the Earth. Since each side panel views only half of the Earth, they will each receive energy equal to half of that which the Earth facing (-Z) surface receives. The equilibrium temperature of the craft when the 'inner' surfaces do not absorb or emit is 310°K. This temperature is higher than the ideal 300°K, but would still be survivable for most space qualified electronic systems.

The coldest orbit on average, is the orbit which has the maximum eclipse. This occurs when the sun is in the orbit plane. Due to the large mass of the payload boxes for inertial requirements, the electronics will remain close to an orbital average temperature throughout the orbit. For the maximum eclipse orbit the average temperature is 281°K which would be ideal for the electronics.

VI.2. Split Geometry

Due to the long vertical member between the payload halves, the +Z and -Z portions of the spacecraft may be more accurately described as thermally independent. In this

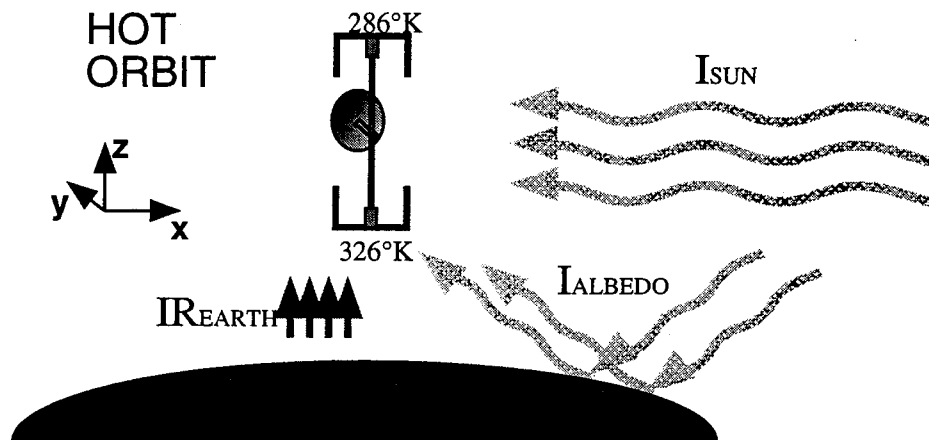


Figure VI.2: Hot Orbit Arrangement: No Eclipse Occurs

model, the two halves of the spacecraft will be separated, and each will serve as an independent entity for thermal purposes. All modes of heat transfer between halves will be neglected. The inner surfaces are still considered to have no effect, and the surfaces within each half are considered to be at equilibrium. The same cases viewed above will be reexamined to see if conditions are still adequate for the survival of the craft. In the full-sun orbit, note that the now split side panel will be exposed to the sun for the entire orbit. Figure VI.2 demonstrates the arrangement of the satellite relative to the Earth horizon. As before, the sun facing (+X) and the opposite (-X) side will see half the Earth exposure of the Earth facing -Z face. The top (+Z) surface will face deep space throughout the orbit. For the Earthward (-Z) half of the satellite, the equilibrium temperature is 326°K . This is likely to be beyond the operating range of the electronic components and would probably cause a failure. Note that this is still within an acceptable temperature for the arrays themselves. The space pointing (+Z) half remains at an acceptable 286°K .

For completeness, the maximum eclipse orbit leads to a colder average temperature for each portion. The sunward and deep space facing (+Z) portion cools to an average of 275°K , while the Earth facing (-Z) section raises slightly to 289°K . These temperatures are very similar to the average obtained by the connected model, and remain within comfortable

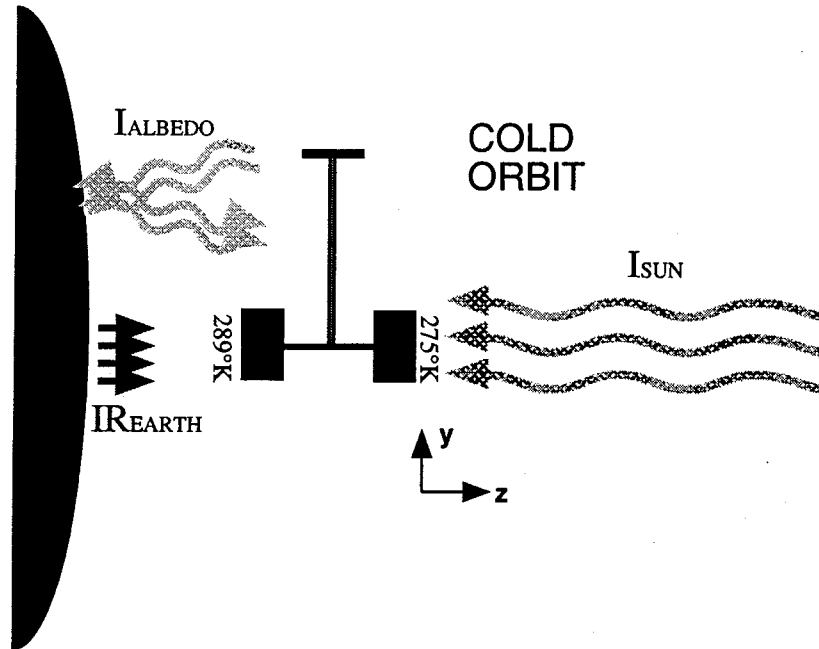


Figure VI.3: Cold Orbit Arrangement: Maximum Eclipse Occurs

operating conditions for the electronics. Figure VI.3, shows the alignment of the spacecraft. With the caveat that the payload masses are sufficient to maintain electronics temperatures near the equilibrium condition, there is no concern in the maximum eclipse orbit. Clearly the difficulty arises in the full sun alignment where the spacecraft overheats. The next section discusses a possible solution to the problem.

VI.3. Partially Deployed Geometry

One possible solution to the overheating of the Earthward side, is to not deploy the solar array on that side. This reduces the surface exposed to the Earth by half, as well as realigning a portion of the array to face deep space. The net effect is to reduce the temperature of the Earthward section to $300^{\circ}K$ which is ideal.

Figure VI.4 shows the satellite in the half deployed configuration; additional information regarding the deployment mechanism is given in section VIII.3. The first

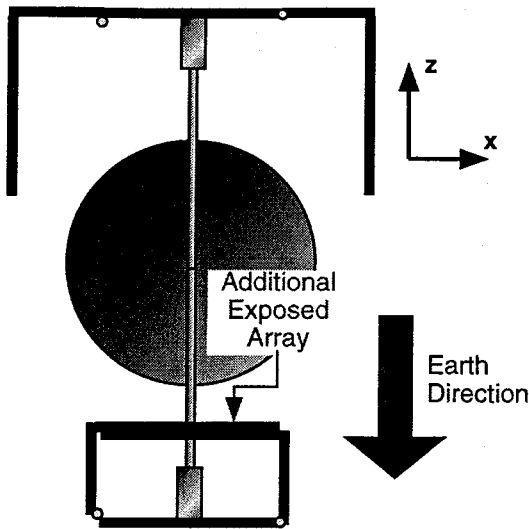


Figure VI.4: Half Deployed Configuration

concern with this arrangement is assuring that enough power is generated for the spacecraft. When the spacecraft orbit is perpendicular to the sun line, the side arrays generate the most power. That is, the sun vector is within 23° of the orbital plane (depending on the time of year). It is advantageous that this configuration allows sunlight throughout the orbit. With only 75% of the array exposed, the total generated power is 65 Watts. Recall

from Chapter V that the maximum power used is 40W with all systems operating. There is over 1.5 times this much power available in this configuration. This extra energy will be used for battery conditioning. Note that in the folded configuration, the spacepointing (+Z) panel on the Earthward (-Z) portion of the satellite will now be fully exposed until the sun is within 23° of the spacecraft Z axis.

The stowed geometry reduces the array area exposed to the Earth by half. Although this affects absorption and emission equally, the improvement is related to the now zenith pointing array surface. The external surfaces are able to emit energy, but also must absorb Earth IR and albedo transmission. The internal, zenith pointing, array is able to emit energy but does not receive energy from the Earth. In effect, the absorbing surface is reduced by half, but the emitting surface is only reduced by 25%. The view of the panel contains the remainder of the satellite, so the reduction is actually slightly smaller. To be conservative, results consider the zenith pointing (+Z) surface of the lower (-Z) half of the satellite reduced by 30%. The new equilibrium temperature is ideal, at 300°K . The arrays make a small contribution to the spacecraft inertial properties relative to the large payload

mass. This configuration will not affect the spacecraft dynamics within the accuracy of the simulations.

The hot condition has been corrected, but this may lead to cold conditions when the sun lies in the orbit plane. Using the same analysis as before, an average effective area for the zenith pointing 'inner' array is calculated. Noting that the inner array is occulted when the sun angle is less than 23° (0.4 radians) the equation becomes:

$$A_{EFF} \approx \frac{\int_{0.4}^{\pi/2} A \cos(\psi) d\psi + \int_0^{0.4} 0 d\psi}{\pi/2} \approx 0.4A$$

Analyzed as separated portions, only the Earthward section changes due to the new configuration. The equilibrium temperature for the stowed lower section is 290°K which is identical to the value for the deployed section in this orbit. Recall that the upper section reached equilibrium at 280°K .

It appears that allowing the outer array to deploy while retaining the stowed configuration for the lower array resolves the overheating concern. It has also been shown that keeping the array in the stowed position will not be a detriment to the cold orbit conditions. It is likely that the addition of a zenith pointing array will increase available power as the sun approaches the orbit plane. Once the sun is within 23° of the orbit plane, the sunward array will begin to occult the inner array. At 16° , half the inner array will be covered (eclipsing one entire solar cell string). Power will quickly degrade as the final string begins to be occulted. This is not a concern for an overall power standpoint since the satellite is designed to operate without this additional power. It will allow additional margin when the satellite is at mid-latitude since the inner array will be exposed at latitudes

above 23° . Note that the actual latitude where the string is eclipsed will vary by 23° due to the seasonal effect of the Earth's axial tilt.

VI.4. Remaining Issues

Clearly this is a simplistic approach to the analysis, and does not involve the transient effects of the operating electronics. For these models, all energy is taken to be absorbed and emitted at the solar arrays. It is assumed that ample conduction will allow the electronics to remain at equilibrium with the arrays. This allows the conclusion that since the array temperatures remain within acceptable ranges for the electronics, the electronics are protected. Internal heat generation has been neglected since without electric generation at the arrays, the arrays reach the temperatures modeled here. Transmission of that energy electrically simply transfers the heat source from the array to the electronic component.

It is likely that there will be local heating spikes due to internal power dissipation. The transmitter will be especially susceptible to heating due to relatively high power needs. Internal analysis of the spacecraft will be necessary including an examination of particular components. Since the arrays have sufficient ability to emit the incoming solar energy, as long as energy transmission paths are available, the electronics should remain within acceptable temperature ranges.

VII. Attitude Control & Stability

One of the primary concerns in developing a mechanical wind measuring satellite, was the ability to control the motion. It is desirable to minimize the frontal area for drag purposes while maximizing the torque for wind measurement. To be successful it is necessary to examine the forces which act on the satellite and attempt to use them to the benefit of the mission. This design will seek to minimize those that can't be controlled. Primarily, the craft is subject to gravity gradient and aerodynamic torques. Secondary inputs include solar pressure and electromagnetic torques. Besides identifying and designing with these inputs in mind, it is important to examine the system dynamics to ensure that the system remains stable.

The stability analysis will show that damping systems will be required to settle the spacecraft motions. In pitch and roll, this can be achieved by conventional fluid ring damping devices. Any attitude rates in these directions will be caused primarily by initial orbital insertion. Some pitching torque may be caused by deployment or construction errors in the tail plate, so this must be carefully controlled. The yawing motion of the satellite will be driven by the variation of the zonal winds. It is the goal of the mission to return this motion as science data. The resulting yaw rates are extremely low ($\sim 70 \times 10^{-6}$ radians/sec), on the order of the rotation rate of the Earth. At this low rate it will be difficult to obtain a satisfactory damping device since most (if not all) current fluid dampers act as solid bodies under these low rotations. Some possible solutions to this problem will be identified at the end of this chapter.

VII.1. Gravity Gradient

The gravity gradient torque arises due to the change in gravitational attraction over the volume of the spacecraft. Since the center of mass (C/M) of the satellite, will orbit the Earth at a speed fixed by orbital mechanics, the other portions of the satellite will be forced to move at the same velocity. Because the spacecraft has distributed mass, portions of the craft will be at different distances from the Earth causing varying gravitational forces throughout the craft. The net result is that the spacecraft tends to orient with the minimum inertia axis aligned with the Earth. A detailed explanation of gravity gradient torques can be found in the References [2,16,17].

To use the gravity gradient to stabilize the satellite, the spacecraft inertial properties must be tailored to particular specifications. Primarily, the axis of minimum inertia will be aligned with the Earth vector. Consider this minimum moment to be about the body z-axis

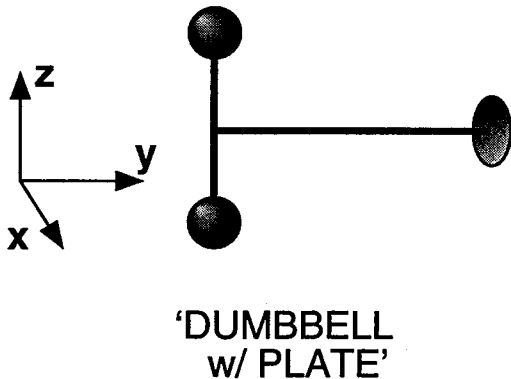


Figure VII.1: End Plate Configuration

(Figure VII.1). Aligning the minimum moment in this way will uncouple the gravity gradient and drag torques. To maximize the lifetime, the drag should be minimized along the relative wind direction. This is possible for the payload portion of the spacecraft and the solar panels, but the tail plate will not satisfy this condition. It is desirable to allow rotations about the z-axis to be caused by changes in zonal wind speed. This yaw motion will be maximized by increasing the aerodynamic drag torque. The inertia requirement can be satisfied with the mass properties of a cylinder or a dumbbell, while the area requirement implies thin members in the y-z plane. Note that the minimum drag direction is not constrained by the mass distribution described above.

With the minimum inertia axis in the desired vertical direction, gravity will align the spacecraft in the desired orientation. Without a damping mechanism, an oscillating system is created. Fluid ring dampers have been employed for damping gravity gradient oscillations, and are readily available for this purpose. These mechanisms consist of a fluid contained in a circular ring and could be located anywhere in the spacecraft. As the spacecraft (and the ring) rotation rate changes, the change is transferred through friction to the internal fluid. Viscosity causes friction in the fluid flow which leads to an energy loss. The fluid will eventually come to equilibrium with the ring when the rotation rate is constant. Note that the fluid motion is caused by angular acceleration, and not angular rate. Since the gravity gradient will align the dumbbell with the zenith, this will control both pitch and roll. Since the spacecraft is symmetric about the y-axis that the satellite may align with either side facing the Earth. This roll ambiguity will lead to redundancy in orientation specific components such as the GPS and radio antennae.

VII.2. Aerodynamics

The aerodynamic design of the satellite seeks to optimize the torque created by the drag without shortening the satellite lifetime beyond a useful range. Recall that a density of $1.916 \times 10^{-11} \text{ kg/m}^3$ is used for all calculations and the effect of increasing density with orbital decay is not considered. This increased density will lead to a larger aerodynamic torque relative to the system damping. Essentially, the system stiffness will increase throughout the lifetime of the spacecraft. Two distinctly different design approaches have been examined in detail and each will be discussed separately in this section. Recall that the elimination of the inline tail design was discussed in the Chapter III. The reasons for this decision will be discussed in detail in the following section to provide comparison for the analysis of the end plate configuration.

VII.2.1. Large Inline Tail Configuration

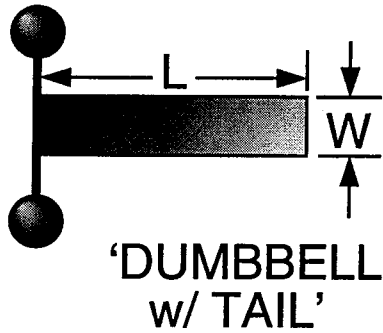


Figure VII.2: Inline Tail Configuration

Since it is the dynamic response which prevents the inline tail from being a viable alternative, this configuration will be discussed for comparison with the end plate design. Figure VII.2 shows the layout for the inline tail concept. To create a large surface area, but keep inertia to a minimum, two or more deployed rods will support a thin membrane. The forces acting on the tail are small enough that 2 mm diameter copper wire is more than sufficient to support the loading.

A 1 mil thick film, made of an oxygen resistant polymer can be used to form the control area. To maximize the response, the ratio of torque to inertia was examined. It is clear that maximizing the area, while keeping the inertia low leads to the best response. Physically, this corresponds to a tail with small length (L) and large width (W). This arrangement also shortens the baseline length for the GPS attitude measurement which is not desirable.

Recall from Chapter III and Figure II.1, that the torque relationship for small angles of attack (α) for the flat tail was given by:

$$T_{TAIL} = \frac{1}{2} C_D \rho v^2 A_{TAIL} R_{CP} \alpha^2$$

Clearly, the air density (ρ) and orbital velocity (v) will not be affected by the physical configuration. The drag coefficient (C_D) will be considered constant for small changes in α . It is mechanically advantageous to attach the membrane to the vertical member of the spacecraft bus as shown in Figure VII.2. This causes the length of the moment arm (R_{CP}) to be half of the tail length (L). Furthermore, the length and the area of the tail (A_{TAIL}) are directly related by the width(W). Rewriting the relationship results in:

$$T_{TAIL} \propto WL^2\alpha^2$$

Note that the rotational inertia of the spacecraft is also related to the length of the tail boom by the following relationship:

$$I_{TAIL} = \frac{WL^3}{3} \left(\rho_A + 2 \frac{\rho_L}{W} \right)$$

where the linear density of the supporting members (ρ_L) and the area density of the membrane (ρ_A) are controlled by material specifications. It is the ratio of the torque to the inertia that must be maximized. When combined, the following relationship is obtained for the angular acceleration:

$$\frac{T_{TAIL}}{I_T} \propto \frac{\alpha^2}{L \left(\rho_A + 2 \frac{\rho_L}{W} \right) + I_0}$$

where I_0 is the moment of inertia of the dumbbell portion of the spacecraft. For lengths greater than 7 meters, I_0 is less than 10% of the total inertia (I_T) and will be neglected.

For any given set of materials, it is clear that the acceleration is inversely proportional to the length. In addition, when the width becomes large, the effect of the structural members is lessened. For the maximum response, the tail would be very short (small L) and wide (large W). The attitude measurement, however, relies on the baseline in the y direction for pitch resolution. This shows that for the ideal mechanical configuration, the attitude measuring ability is minimized leading to a design tradeoff.

Note that the acceleration is proportional to the square of α . For the majority of the spacecraft lifetime, the wind angle relative to the orbit plane is less than 35 mradians (2°). At this maximum, α^2 is approximately 0.001. Compare this with the desired resolution of

10 m/s. A 10 m/s change in zonal wind leads to a change in relative wind angle of 1.3 mradians for an α^2 of 1.7×10^{-6} . To develop an ideal response the spacecraft must respond to all wind angles between 1 and 35 mradians. The ratio between torque and inertia can not be optimized for the three order of magnitude range of α^2 . The following simulation results will demonstrate how this affects the attitude response of the spacecraft.

A sample wind profile with a high speed gradient at the north pole, and a smaller gradient at the south pole was used for simulation purposes. This profile was obtained from a contour plot of wind speeds [18, Figure 5] and is valid as a realistic example only. The simulation corresponds to one polar orbit of the satellite- from the equator, across the north pole, south to the south pole, and back north to the equator. In Figure VII.3, the wind angle is shown with a dotted line, and the spacecraft response with a solid line. Note how the spacecraft fails to respond to the small changes in wind direction, missing the details of the profile curve. There is also significant lag; this is partially due to the inability

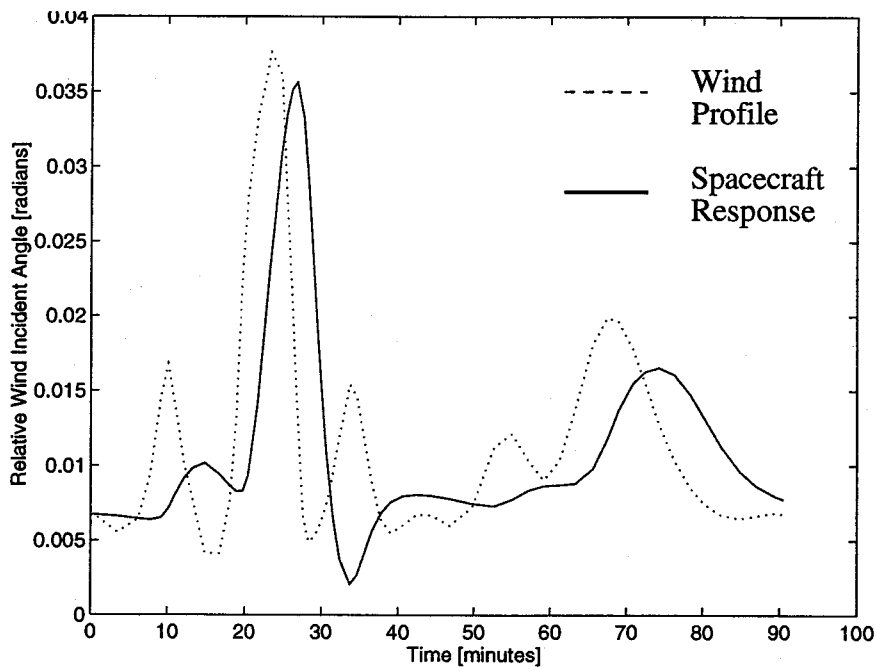


Figure VII.3: Satellite Response for Tail Configuration

of the craft to respond due to the α^2 relationship. The remaining lag is due to rate proportional damping. Since it is the goal of the mission to measure the global wind patterns, failing to detect small changes is unacceptable. The end plate design does not have this same shortcoming, but will have a shorter lifetime. An extended lifetime is not advantageous if the measurement resolution is not an addition to current knowledge. Therefore, the end plate design has been chosen for this mission.

VII.2.2. Tail End Plate Configuration

This configuration differs only in the tail design. The solar panels, and payload boxes remain the same. For aerodynamic response, a boom is deployed with a perpendicular plate at the end. The drag on the plate acts on a moment arm to provide the necessary torque as in the flat tail approach. In this case, however, the frontal area is not minimized at equilibrium. In fact, the majority of the spacecraft area is due to the plate itself. Again, the ideal mechanical configuration leads to a short tail boom. If a balance can be reached where the system response is on the order of the measurement resolution, then an optimum solution can be obtained. A lifetime estimate can be obtained for each solution, resulting in a relationship between mission life and measurement accuracy.

Again, recall the torque relationship from Chapter III for the tail end plate design. With the small angle approximations the equation is:

$$T_{PLATE} = \frac{1}{2} C_D \rho v^2 A_{PLATE} R_{CP} \alpha$$

Recalling that C_D , ρ , and v are independent of the mechanical nature of the craft, and that R_{CP} is equal to the length of the boom (L):

$$T_{PLATE} \propto A_{PLATE} L \alpha$$

The rotational inertia of the tail is a function of A, L and the component densities as before:

$$I_{PLATE} = \frac{L^2}{3} (\rho_L L + 3\rho_A A_{PLATE})$$

Examining the ratio of the two, the acceleration is proportional to:

$$\frac{T_{PLATE}}{I_T} \propto \frac{\alpha}{L \left(\rho_L \frac{L}{A_{PLATE}} + 3\rho_A \right) + I_0}$$

where I_0 is again the moment of inertia of the spacecraft bus and I_T the total spacecraft inertia. In this configuration I_0 is not ignorable, but is controlled by payload and lifetime requirements.

It is obvious that for the greatest response, the plate area needs to be maximized and the tail length and mass minimized. In addition, it is clear that the acceleration is directly proportional to the angle of attack. This leads to the equation of a harmonic oscillator for the spacecraft yaw angle.

$$I_T \ddot{\theta} + C \dot{\theta} + K \theta = K \gamma(t)$$

$$\text{where } I_T = I_z \approx I_0 + \frac{L^2}{3} (\rho_L + 3A_{PLATE} \rho_A)$$

$$K = \frac{1}{2} C_D L A_{PLATE} \rho v^2$$

$$C = 2\zeta \sqrt{K I_T}$$

where $\gamma(t)$ is the incident wind angle as a function of time. The angle of attack α , is the difference between the spacecraft yaw angle (θ) and γ measured from the orbital plane. $\gamma(t)$, α , and θ are shown in Figure VII.4.

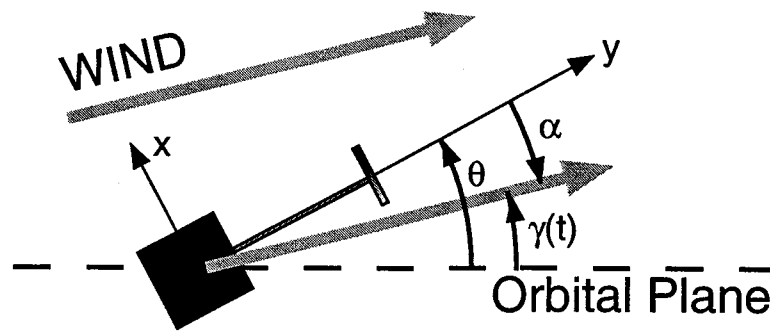


Figure VII.4: Relationship between α , γ , and θ

To determine the design values of the various system parameters, a MATLAB numerical simulation was used. Although the actual method of damping has not yet been established, the optimal dimensionless damping ratio (ζ) can be found through simulation. This damping corresponds to an ideal system which provides damping proportional to the spacecraft yaw rate. Realizing that the plate area is the leading factor in orbital lifetime estimations, a minimum lifetime bounds the maximum plate size.

From dynamic simulations, a time average of the wind tracking error can be developed. This average tracking error is used to rate system performance for various tail lengths and ζ . The phase measurement limitation of the attitude device relates the baseline length to this average tracking error. An ideal tail boom will provide sufficient baseline for yaw angle solutions on the same order as the average tracking error obtained. An iterative search on tail length was used to find this ideal dimension. Once this iteration converged, ζ was added to the optimization. Certainly, varying ζ will alter the ideal length so further iteration must include both length and ζ .

A design space was established in three parameters; area of the plate (A_{PLATE}), tail length (L), and damping ratio (ζ). A search of this space was performed to find the minimum tracking error for a given plate size. L was constrained by the GPS antennae

baseline required to achieve a wind speed resolution equal to the average tracking error for that configuration. Therefore the GPS attitude device would be capable of a measurement at least as precise as the wind tracking ability of the spacecraft. After a minimum tracking error was found for each plate size, it was determined that tracking error was inversely related to plate area. This relationship was used to define a design trade.

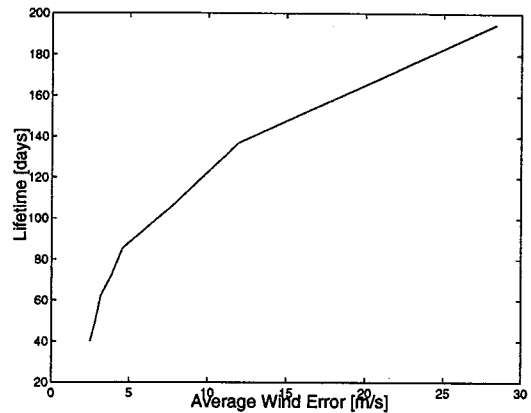


Figure VII.5: Lifetime Vs Average Wind Measurement Error

The design trade involves measurement accuracy and satellite lifetime. Lifetime is defined for this mission as the time necessary for the spacecraft orbit to decay from 300 km to 200 km altitude. The frontal area of the spacecraft bus is fixed by the payload and solar panels, therefore the lifetime is driven by the plate area. For a phase determination within 1 mm, Figure VII.5 shows the relationship between the expected orbital lifetime and the average measurement error. Recognize that the plate area is inversely related to both the error and the lifetime. For a three month lifetime, the plate area is limited to 0.36m^2 . At this size, the average angular error becomes 0.7 mradians. This is equivalent to a wind measurement within 5 m/s. This was obtained with a boom length of 1.5 meters, and ζ equal to 0.2. System response is shown in Figure VII.6, and is obviously improved from the flat tail configuration. It is, in fact, difficult to distinguish between the system motion and the wind profile for the majority of the orbit. A few particular aberrations are worth noting.

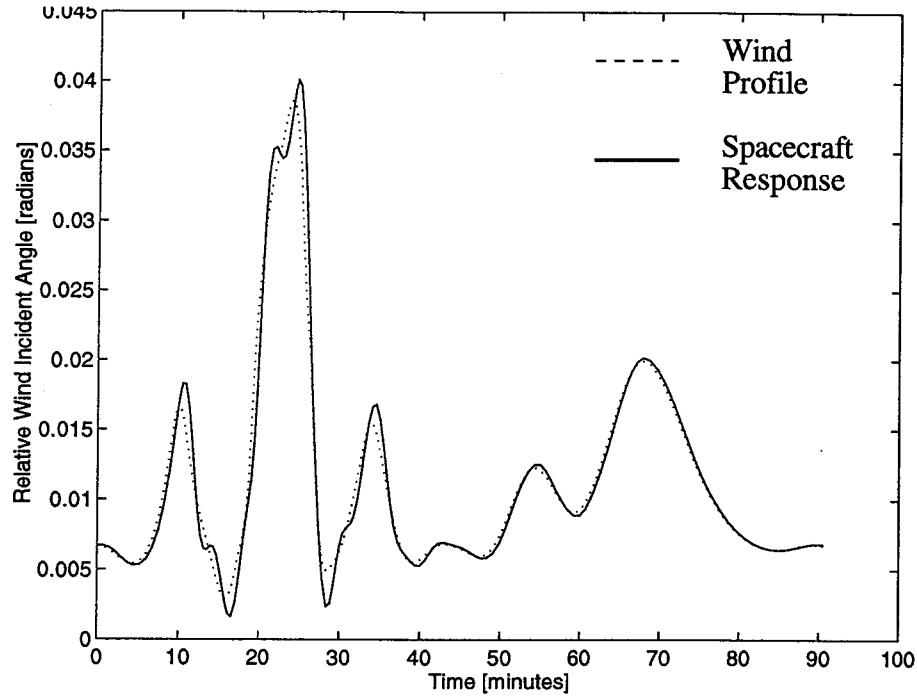


Figure VII.6: Tail End Plate System Response for a 3 Month Lifetime

An overshoot oscillation is apparent during the downward turn at $t=15$ minutes, as well as near the peak at $t=22$ minutes. This is due to the relatively steep slope of the wind profile in these areas. Since $\zeta=0.2$, some overshoot and oscillation is to be expected. Overshoot responses are also clear at the top of the peak, and at the base of the primary peak. A slight lag is apparent due to the linear damping, but since the system is a linear harmonic oscillator, it may be possible to predict the average system lag.

Recall that these results are based on a 1 mm phase detection. As the phase determination becomes less accurate, a longer boom is required. Since it has been shown that system acceleration is inversely proportional to length, this would lead to a slower system response. This would, in turn, force larger angular errors.

VII.3. Damping Methods

Because the yaw rates are so small, it will be difficult to construct a damper that will have sufficient energy loss. Conventional dampers include fluid filled rings and magnetic hysteresis rods. Another method that may be acceptable for this mission is increased structural damping in the form of viscoelastic members. Active damping through the use of magnetic torque rods may also be possible by making an angular rate estimation from the attitude measurements.

VII.3.1. Fluid Ring Dampers

Fluid dampers are generally used in higher rate applications. Damping initial kickoff tumble and nutation damping in spin stabilized satellites are two particular examples. A fluid ring damper utilizes the shearing friction on the inner wall of a tube of fluid. Figure VII.7 shows a representative sketch of a simple fluid ring damper. Note that the fluid resists the angular acceleration of the ring through viscous friction. It is the inertia

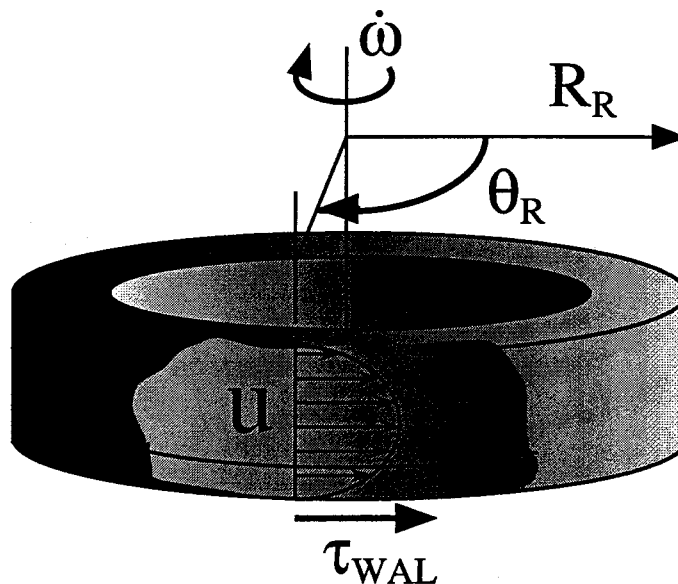


Figure VII.7: Fluid Ring Damper

of the fluid which leads to relative motion between the fluid and the ring. As the ring is accelerated, the fluid lags, leading to a velocity distribution (u) as shown in the diagram. The energy dissipation will be a function of the kinematic viscosity and the acceleration. For this low rate application, a fluid with a high density and low viscosity is desired.

For a circular ring with circular cross section (versus the rectangular section above), the equation for the velocity profile as a function of time was found for a periodic input. This periodic input would correspond to an angular oscillation about the axis of the ring. A small segment of the tube may be approximated as laminar flow in a straight pipe. This flow is symmetric about the center of the tube, and independent of angular position about the ring (θ). With these assumptions, the Navier-Stokes equations [19, Equation 6.71] for incompressible viscous fluid flow become:

$$\frac{\partial u}{\partial t} - \nu \left(\frac{\partial^2 u}{\partial r^2} + \frac{1}{r} \frac{\partial u}{\partial r} \right) = 0$$

with the following boundary conditions:

$$u(R, t) = U_0 e^{-i\Omega t}$$

$$\frac{\partial u}{\partial r}(0, t) = 0$$

where r is the radial position from the center of the tube, R is the radius of the tube, ν is the kinematic viscosity, Ω is the periodic frequency, u is the velocity, and U_0 is the maximum wall velocity. By using a periodic input, the time dependency can be removed, and the equation reduces to an ordinary Bessel's equation of the first kind of order zero. The resulting function of velocity versus tube radius and time is:

$$u(r, t) = \text{Real} \left(U_0 \frac{J_0(\beta r)}{J_0(\beta R)} e^{-i\Omega t} \right)$$

$$\text{where } \beta = \sqrt{\frac{\Omega}{2\nu}} (1 + i)$$

The force transmitted to the spacecraft is equal to the wall shear stress multiplied by the inner surface area of the tube. Shear stress at the pipe wall is given by:

$$\tau_{\text{WALL}} = \mu \left. \frac{\partial u}{\partial r} \right|_{r=R}$$

where μ is the fluid viscosity. The viscosity (μ) and the kinematic viscosity (ν) are proportional and related by:

$$\nu = \frac{\mu}{\rho}$$

where ρ is the density of the fluid. Note that at these rotation rates all flow is laminar. As a result wall roughness does not affect the fluid flow or wall shear [20]. The peak force on the ring wall, and the moment about the ring axis are then:

$$F_{\text{RING}} = (2\pi R R_R)^2 \mu \left. \frac{\partial u}{\partial r} \right|_{r=R}$$

$$M_{\text{RING}} = R_R (2\pi R R_R)^2 \mu \left. \frac{\partial u}{\partial r} \right|_{r=R}$$

where R_R is the radius of the ring.

From the wind profile shown previously in Figure VII.3 and Figure

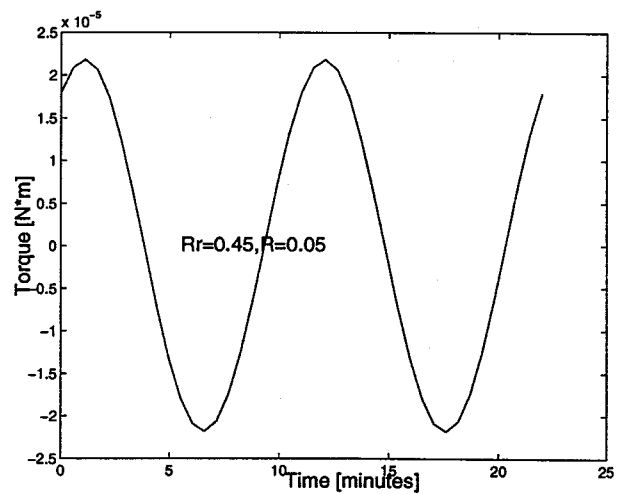


Figure VII.8: Large Ring ($R_R=0.45\text{m}$): Damping Torque Vs. Time

VII.6, an oscillation can be observed with a period of approximately 11 minutes. This is approximately one eighth of the orbital period. Using a period of 11 minutes, an estimate of the ring torque was obtained for mercury as a working fluid. Mercury has a viscosity (μ) of 1.8×10^{-3} kg/(m-s), and a kinematic viscosity (ν) of 0.15×10^{-6} m²/s. Mercury is used due to its high density and low

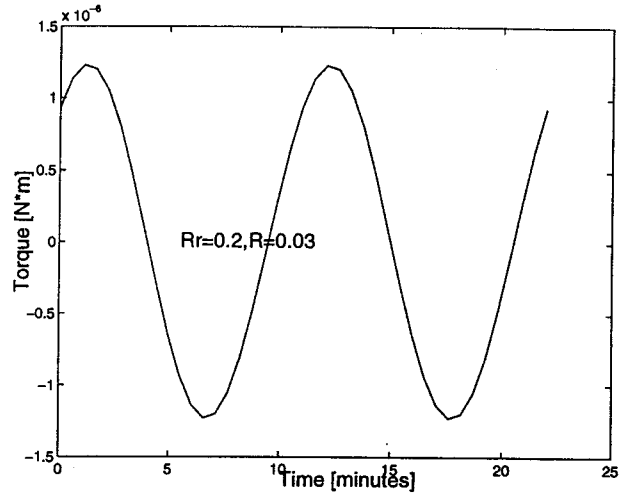


Figure VII.9: Small Ring ($R_R=0.20$ m): Damping Torque Vs. Time

viscosity. Figure VII.8 shows a plot of the torque provided by this theoretical damping ring versus time. The maximum torque provided by the ring is 22×10^{-6} N-m. This is approximately half the magnitude of the torque provided by the wind. This would be sufficient for damping purposes, but at an outer radius (R_R) of 0.45 meters; the ring is as large as the 0.9x0.9 meter upper solar array. This would require the damper to fold with the stowed array. The tube radius (R) is limited to one order below R_R by the straight pipe assumption used to develop this fluid velocity model. Limiting the ring size to the dimensions of the folded array ($R_R=0.2$ m) leads to Figure VII.9. Now the maximum torque is 1.3×10^{-6} N-m. This is 2.4% of the maximum wind torque (55×10^{-6} N-m) and would be equivalent to $\zeta=0.012$ for a periodic system. Recall that for the response shown in Figure VII.6 ζ was equal to 0.2. Without a means to generate a larger damping torque, another method will need to be employed for yaw rate control.

A dynamic simulation of the system including the effects of the ring damper was not performed due to the results of the analysis shown above. It may be a revealing analysis, but would involve the added complexity of numerically integrating the velocity

profile throughout the simulation. This was decided to be beyond the scope of this investigation.

VII.3.2. Magnetic Hysteresis Dampers

Magnetic hysteresis dampers use the Earth's magnetic field to dissipate energy. Mechanically, a magnetically 'soft' material is formed into a rod perpendicular to the axis where damping is desired. As the rod moves relative the magnetic field, the material's microscopic structure attempts to align with the field. Since the microstructure is slow to respond, the residual field created by the rod creates a torque that resists the motion. Over time the rod will align with the field lines in the absence of other forces. The rod never reaches equilibrium however, since the orbital motion causes a periodic change in the local field direction. This leads to a disturbance torque with a period that is a multiple of the orbital rate. When the spacecraft rates are small relative to the orbital rate such as in this mission, this disturbance becomes significant. This method is effective for removing initial kickoff tumble, but is not appropriate for missions sensitive to orientation.

VII.3.3. Viscoelastic Damper

The use of viscoelastic structural materials, such as a rubber, is another damping approach. One particular method would involve placing a rubber section between the tail boom and the spacecraft body. This would cause energy dissipation as the tail moves relative to the dumbbell section of the craft. The analysis of viscoelastic materials can become highly complex, but a simplified model was developed as shown in Figure VII.10.

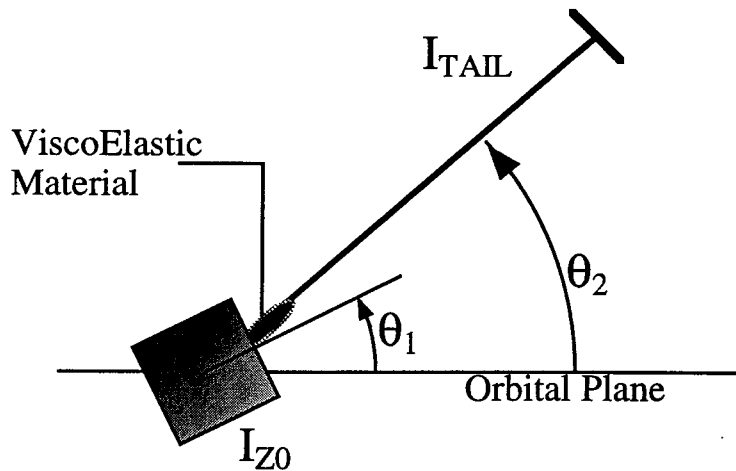


Figure VII.10: Model Of Viscoelastic Damper for Satellite Dynamics

This simplified model includes a linear spring of stiffness K , and a linear viscous damper of resistance C . Note that it is the relative motion of the tail with respect to the dumbbell that is damped. The simulation results given earlier in the chapter used a damper which was proportional to the solid body motion of the entire spacecraft. The equations of motion for the new two degree of freedom system become:

$$I_0 \ddot{\theta}_1 - C_v (\dot{\theta}_2 - \dot{\theta}_1) - K_v (\theta_2 - \theta_1) = 0$$

$$I_{TAIL} \ddot{\theta}_2 + C_v (\dot{\theta}_2 - \dot{\theta}_1) + K_v (\theta_2 - \theta_1) + K \theta_2 = K \gamma(t)$$

where Spring Constant of V.E. material $\equiv K_v$

Damping Coef. of V.E. material $\equiv C_v$

$$K = \frac{1}{2} C_D \rho v^2 A_{PLATE} L$$

This formulation neglects the wind effect on the dumbbell section of the spacecraft. Using these linear equations in MATLAB allowed a design space search similar to the one performed before. The resulting spring and damping coefficients for a 1.5 meter long boom are $K_v=0.001$ N-m/radian and $C_v=0.0035$ N-m-s/radian. A plot of the corresponding case using the nonlinear model to include the wind effect of the dumbbell portion is given in Figure VII.11. This model uses linear damping and spring coefficients

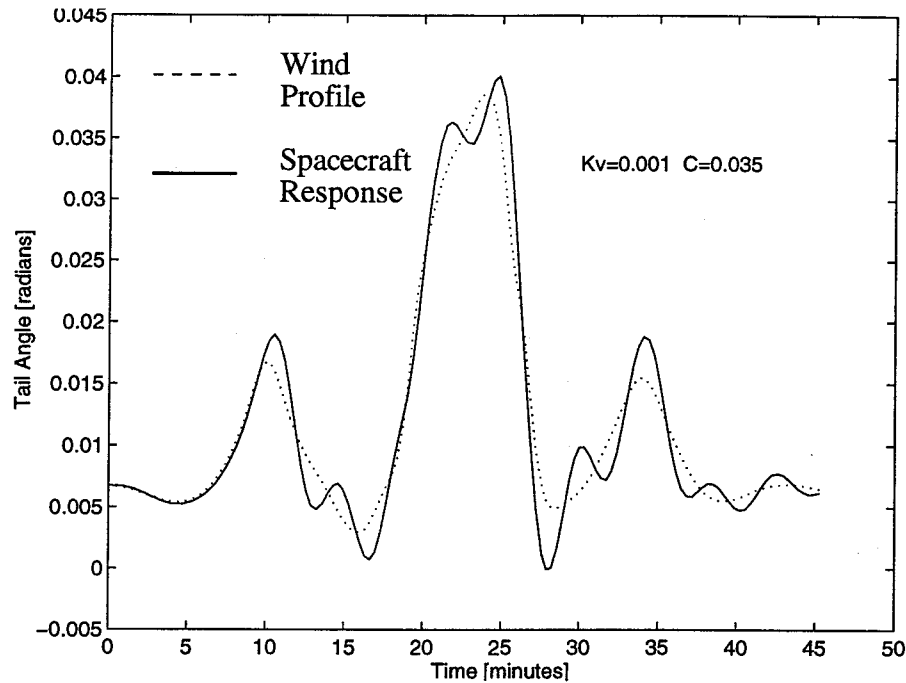


Figure VII.11: System Response With Linear Viscoelastic Mechanism at Tail Boom Junction

without regard to actual materials. Generally, actual viscoelastic devices act in a material specific, nonlinear fashion, so it is unclear whether materials can be found that would have these characteristics. Experimentation at the rates involved in this experiment would be necessary to determine an appropriate material. Angular springs and dashpots are a similar approach which would provide linear responses, but have not been examined.

VII.3.4. Active Damping

Although the purpose of this analysis was to examine passive methods of reaching the mission goals, it is worth mentioning that active damping techniques might be satisfactory. One method would use a state estimator to develop a model for the spacecraft motion. Essentially, a numerical derivative will be evaluated based on the attitude data generated by the GPS. Using the estimated derivative, an active system, such as magnetic torque rods, could be used to counter the rotational velocity. The goal would be to generate

a torque proportional to the angular rate that opposes the motion. An ideal controller will generate a damping torque identical to the $C\dot{\theta}$ term in the linear equation of motion. The energy expense for the torquing system is negligible relative to the other electronics. However, additional computational power would be required to maintain an attitude estimate, and to perform the necessary angular rate calculations. Implementation of the torque rod controller would consist of a simple derivative feedback system. A high order magnetic field model or magnetometer would be required to determine the strength and direction of the necessary magnetic moment. Note that if active control methods are used, data concerning the control torques would need to be stored and downlinked in addition to the attitude information. This would be necessary to calculate the input function versus time. It is the aerodynamic portion of this input function which relates to the desired science data.

VII.4. Solar Torque

There are two alternatives for the tail plate design that serve to minimize the solar pressure effects. For a tail plate made of a reflective material, the maximum deflection caused by the solar pressure is 7.7 mradians (0.44°). This represents the worst possible material choice and spacecraft orientation. Since the 0.36 m^2 plate is still an order of magnitude larger than the projected area of the rest of the satellite at this angle (0.061 m^2), the small bias does not affect the orbital lifetime due to increased drag. The attitude effect of sunlight on the surface of the spacecraft would need to be modeled based on the optical properties of the exposed materials and the position of the sun. This model would be used to remove the bias caused by the solar input. If prediction of the solar influence is not possible within the wind measuring resolution, the solar effects can be minimized through the use of a transparent material for the plate surface. This alternative would lead to a solar

deflection of 0.38 mradians for a 90% transparent plate. Since the bias is smaller than the measurement resolution of the spacecraft, solar effects would be ignorable. Either alternative is within current technology if an optical model of the spacecraft can be created. Because the end plate will be pointing into the velocity, or ram, vector; the end plate material must resist degradation due to impacting high energy particles.

Atomic oxygen in particular leads to deterioration in polymer films. At least one transparent film is available commercially [21] which exhibits atomic oxygen resistance sufficient for use on the end plate. This film exhibits 95% transparency to solar input. The plate would then consist of a rigid structure supporting a film of this or another resistant material.

VII.5. Remaining Attitude Control Issues

In addition to those topics listed so far, there is the possibility that electromagnetic torques will disturb the system. Since the electronic components use power at a variable rate, intermittent magnetic fields may be generated. These could be caused by current loops in the component wiring, or by change in current in linear paths. Any current carrying conductor generates a magnetic field, and it is possible that for the magnitude of the torques involved in this mission that they may be significant. Without a detailed examination of each component, an estimate of this disturbance can not be made. It is sufficient however, to be aware of the disturbance so that an attempt can be made to minimize it. Magnetic field isolation cages could be constructed around some of the electronic devices. These consist of conductive materials which surround the components. This would not be possible in the case of the GPS and radio antennae since they rely on the transmission of magnetic fields. These devices act at frequencies that are too high to be a consideration, however. Careful

circuit design and testing of the overall system is sufficient to prevent these torques from influencing the wind measurements.

From the discussions above, it is clear that additional analysis will be required. At this time it has been established that the system response could be tailored to return sufficient science data. The drawbacks are the shortened lifetime caused by the tail end plate approach and the need for significant damping. Before an accurate feasibility determination can be made, a detailed examination of the damping mechanisms will need to occur. It is likely that there are other damping options which are not introduced in this report, but may hold the key to an appropriate system response. Conventional fluid ring, and magnetic hysteresis systems are deemed insufficient or inappropriate for this mission. Viscoelastic structural members, or specially constructed rotary damping devices may be effective approaches to the desired spacecraft dynamics. If passive approaches prove insufficient, it is possible that active torqueing methods may be an appropriate alternative. Active systems require increased cost in control system design and added general spacecraft complexity. This discussion will now turn to the communications, data handling systems, and other remaining satellite subsystems.

VIII. Communications

For a spacecraft which is not designed for reentry to return data to the Earth, a communications link must be established. For the purposes of this mission radio transmission is assumed based on readily available commercial components. It is possible to analyze the capability of such a link based primarily on the amount of data to be transmitted and the output power of the transmitter. Ground station time in view and availability will affect the required data rate. Ground station viewing by this satellite requires omnidirectional antennae to provide radio coverage without active tracking by the spacecraft. The ground station is assumed to have tracking capability. The following sections contain the analysis of the communications link.

VIII.1. Data Volume and Rate

The communications subsystem is used to transmit status and science data to the ground, receive commands, and store data for later transmission. This system must be sized to handle the quantity of data expected, and the amount of time available for transmission. The transmission time is determined by the Earth horizon of the spacecraft, and the orbital velocity. Both are functions of altitude for a circular orbit. For a 300 km altitude, the time the spacecraft is in view above 5° elevation is 6.5 minutes. Considering that time must be allocated for handshaking and acquisition problems, 5 minutes is a more conservative estimate. Examination of the expected data volume is considerably more approximate than available transmission time since a detailed estimation of the data to be sent is not possible.

The GPS attitude device will return attitude angles and position information as a minimum. It is possible that system status information as well as noise estimates could be returned. For a resolution of 100 meters, each position component would need to be an 18 bit word. For an angular resolution of 0.5 mradian (3.5 m/s wind resolution) in pitch and yaw, two 14 bit words are necessary. Roll is less precise requiring only 13 bits. For status and other information, double the total and raise it to the next highest power of two to get 256 bits per sample.

It is unclear how much satellite status data will need to be added for telemetry and other purposes, but if this is taken as similar in size to the science data the total would be 0.5 kbits per sample. Note that one kbit is equal to 1024 bits. If samples are taken once every 30 seconds, throughout one day 1.5 Mbits will be necessary. In conventional memory terms this is less than 200 kilobytes. Compared to standard computer memory capabilities, this value is small, making storage within conventional technology.

To transmit the data, a ground station must be chosen and daily passes scheduled. Due to the increased loading on ground sites, it is wise to allow the possibility of a missed orbital pass. This would double the storage, and the necessary transmission rate. As an added benefit, data quality would increase because of the likelihood that data could be retransmitted if passes are made daily as scheduled. If 400 kilobytes are to be transmitted in 5 minutes, 11,000 bits per second (bps) will be required. Once a modulation scheme is chosen, a signal to noise ratio can be determined for a given bit error rate (BER). The BER is the probability that any given bit will be received incorrectly. Using binary phase shift keying (BPSK), a common data modulation technique, a signal to noise ratio of 7 dB would allow only one bit error per transmission [2]. The communications link analysis below can determine whether sufficient transmitter power is available.

VIII.2. Link Analysis

Choosing communications components requires the determination of the link budget. This design tool examines various sources of noise, and signal amplification to determine the final signal to noise ratio. The process that follows is taken directly from Larson & Wertz, *Space Mission Analysis and Design* [2].

First, a carrier frequency and transmitter power must be chosen. Generally small spacecraft choose frequencies in the S band (2.5-2.7 GHz). This study will examine power

Item	Units	Uplink	Downlink	
Frequency	GHz	2.3	2.5	
Xmitter Power	Watts	1.0	1.0	
Xmitter Power	dBW	0.0	0.0	
Xmitter Line Loss	dB	-1	-1	
Xmit Ant. Beamwidth	deg.	2	180	Input Parameter
Xmit Ant. Diameter	m	4.57	0.05	
Peak Xmit Ant. Gain	dB	38.3	-0.8	
Xmit Ant. Pointing Offset	deg.	0.2	90	
Xmit Ant. Pointing Loss	dB	-0.1	-3.0	
Xmit Ant. Gain	dB	38.2	-3.8	
Equiv. Isotrop. Rad. Power	dBW	37.2	-4.8	
Satellite Altitude	km	300	300	
Propogation Path Length	m	1.98E+06	1.98E+06	
Space Loss	dB	-165.6	-166.3	
Propagation & Polarization	dB	-0.5	-0.5	
Rec. Ant. Diameter	m	0.05	4.57	
Peak Rec. Ant. Gain	dB	-3.57	36.37	
Rec. Ant. Diameter	m	0.05	4.57	
Rec. Ant. Beamwidth	deg	183	2	
Rec. Ant. Pointing Error	deg.	91	0.2	
Rec. Ant. Pointing Loss	dB	-3.00	-0.12	
Rec. Ant. Gain	dB	-6.57	36.25	
System Noise Temperature	K	1295	552	
Data Rate	bps	1000	11000	
Signal to Noise Ratio	dB	32	25	
Bit Error Rate		100.0E-6	100.0E-6	
SNR Required	dB	10	10	
Implementation Loss	dB	-3	-3	
Link Margin	dB	19	12	

Table VIII.1: Communications Link Budget

needs for a 2.5 GHz transmitter. The transmitter power will be considered for 1 Watt of transmission power. A 1 Watt unit is one of the smallest commercially available satellite transmitters in terms of power. Since the procedure is available in Larson & Wertz, a summary table of important link values is included in lieu of a detailed process.

It is clear from the results shown in Table VIII.1, that due to the low data rates, the single watt transmitter is slightly larger than what is necessary. The link margin corresponds to the amount of power that is available beyond what is required. Approximately 10 dB are generally sufficient to compensate for rain and other unmodeled degradation. If a lower power transmitter can be obtained, it would allow power to be saved. However, since the actual quantity of data to be retrieved is approximate, at this time, the 1 Watt device will be used. It would also be possible to save power by increasing the data rate to shorten transmission time. It is also apparent that the uplink is well within acceptable parameters, due to the large transmission dish, and again, small data rate. From a feasibility standpoint, there are no obvious concerns in the communications subsystem.

IX Other Subsystems

Two remaining subsystems, data handling and deployment systems, are discussed briefly here. Since they do not represent technological challenges for this mission, the analysis is brief. Data handling and control systems provide autonomous capability for the spacecraft. This allows the satellite to monitor regular activities and make adjustments while minimizing the necessary ground interaction and monitoring. This is advantageous due to the high personnel costs involved.

The tail boom will need to be stowed for launch to minimize the required launch envelope. The smaller the satellite is before deployment, the lower the cost to orbit. This is due to the greater availability of small payload spaces aboard launch vehicles versus larger berths.

IX.1. Data Handling and Subsystem Control

Since the spacecraft is simple from a computer control point of view, a detailed analysis of this subsystem was not performed. Instead, a short discussion of the tasks that the controller will need to perform is included. It is assumed that the GPS attitude determination is done internally by the attitude device. This system will have a self contained processor for data analysis, averaging, and perhaps state estimation. The GPS device will output processed data in the form of attitude and position information, sampling rate and statistical data. The central controller will accept this information and route it to a storage device. Considering the low quantity of data, solid state memory chips will be employed to store all onboard information.

In addition to data handling, the central processor (CPU) will monitor the electrical system, perhaps in a regulatory role. Rather than have a dedicated power system controller, the CPU could handle these tasks. Power generated at the solar arrays will need to be regulated, and battery charges maintained. The battery drain will need to be monitored, and systems controlled based on available power. For example, if power is insufficient, it may be possible to skip a transmission and store the excess data until the following opportunity. Even if sufficient storage space is not available, it would be better to lose data than to damage the power cells and jeopardize the future of the mission. Besides the electrical system, the CPU will need to monitor component temperature and deactivate components in unsafe conditions.

Low level attitude information could be obtained based on solar array power levels and used to assist the GPS unit during initial attitude determination. Since voltage is constant over the majority of incident angles, only current would need to be observed. If the amperage can be measured within 5%, the angle between the sun and the solar array normal can be determined within 20°. Between the orthogonal solar panel surfaces, an attitude estimate can be developed that could be used to minimize integer wavelength ambiguity. This would be most useful during initial determination, but would also be helpful if GPS lock is lost temporarily.

These are the primary tasks which are likely to be controlled by a central computer. Sufficient computational power can be obtained without the need for an extremely complex controller. Most calculations are simple comparisons of incoming information with preset thermal or electrical limits. If an attitude estimation is desired, a more advanced processor will be required. Regardless, sufficient controllers are readily available and do not represent a technology limit for the spacecraft.

IX.2. Deployment Systems and Structure

It is advantageous to employ a deployment system to minimize the required payload size for launch. The tail boom can be deployed if strength and stiffness constraints are met to ensure GPS baseline consistency. It is also necessary to be able to fold the solar arrays into a configuration which benefits the spacecraft thermal considerations. The main vertical support may also be extendible if a smaller payload size is necessary. Figure IX.1 demonstrates possible stowed and deployed configurations for the solar panels.

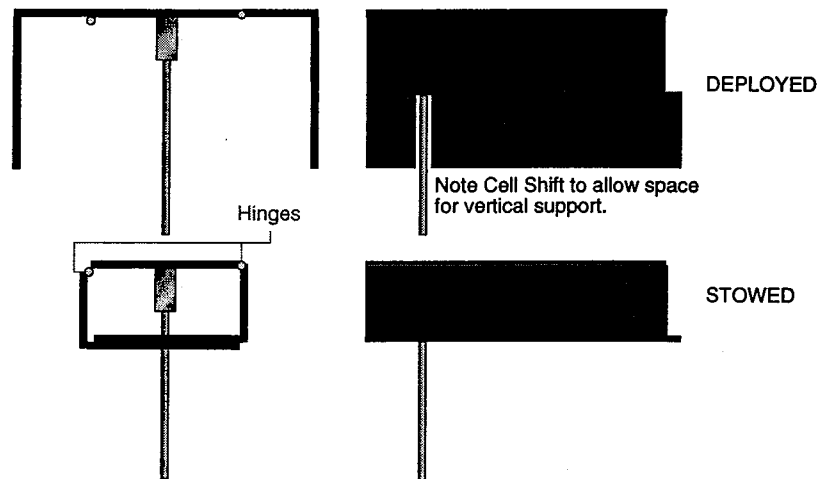


Figure IX.1: Stowed and Deployed Configurations

For the tail construction, several parameters should be closely controlled. Since the length of the tail will be used as the baseline for the attitude calculations, the distance between GPS antennae must be predictable within the 1 mm phase resolution. For proper attitude determination, the direction from the antennae on the main body, to the antenna on the tail must be known within the angular resolution of the attitude device. In addition, the deployment device must support the thin membrane of the tail plate.

This membrane forms the aerodynamic surface which orients the spacecraft. A misalignment in the deploying member or the plate itself leads to a pitching torque or a yaw

bias. The yaw bias would cause wind measurement error and should be minimized. If the pitching torque exceeds the gravity gradient torque, then the spacecraft may begin to tumble. The maximum torque provided by the gravity gradient is $250 \mu\text{N}\cdot\text{m}$, so this bounds the acceptable tail error torque to $250 \mu\text{N}\cdot\text{m}$ for stability. However, stability alone is not sufficient. To maintain the three month orbital lifetime, the average pitch angle must be less than 22 mradians (1.3°). At this value, the area contribution of the bus portion of the spacecraft becomes 10% of the end plate area and significant to lifetime calculations. Any additional pitch will lead to a measurably shortened lifetime. For the current satellite configuration, the gravity gradient torque will provide $11 \mu\text{N}\cdot\text{m}$ of torque at 22 mradians of pitch. The disturbance torque must therefore be less than $11 \mu\text{N}\cdot\text{m}$ to maintain a pitch angle below 22 mradians.

From a strength perspective, it is possible to model the tail as a cantilever beam attached to an unmoving spacecraft. The drag acts like a point load on the tip of the 1.5 meter boom. For the plate configuration simulated in Chapter VII, the maximum torque possible at the support was $340 \mu\text{N}\cdot\text{m}$. This would occur when the yaw angle of attack relative to the wind stream is $\pi/4$ radians (45°). This could only occur immediately after deployment before the satellite aligns with the relative wind. For nominal operations (yaw angle of attack ≤ 35 mradians), however, the reaction moment at the support reduces below $20 \mu\text{N}\cdot\text{m}$. It is necessary to prevent the tail from bending more than the 1 mm phase measurement resolution for nominal loading. This requires a support with a bending stiffness, $E \cdot I$, greater than $0.15 \text{ N}\cdot\text{m}^2$ [22]. This is equivalent to a circular copper ($E=120 \text{ GPa}$) wire with a diameter of 2.3 mm (Brown & Sharp 11 gauge). Deployable “carpenter’s tapes” can be obtained with bending stiffnesses that satisfy the requirements above.

Deployable tapes are generally made of a copper alloy for high thermal conductivity and improved stiffness and strength over copper alone. There are several general approaches to booms of this type: open tube, closed tube, and curved tapes. Example cross sections of each type can be found in Figure IX.2. The open tube is commonly referred to by its trade name, STEM (Storable Tubular Extendible Member). The STEM consists of a strip of spring metal heat treated into an overlapping cylinder. Storage is achieved by flattening the strip and winding it around a drum. The Bi-STEM is an extension of this technology which uses two flat strips on the same drum. These strips form one overlapped cylinder when deployed [23]. The closed tube, or quasi-biconvex tube, is also known by the trade name MAST (Multiple Applications Storable Tube) [24]. It is constructed of two strips which are welded together at the edges such that a void is created at the center. It is also wound about a spool, which causes stressing of the edge welds when flattened. The final variety, and generally the cheapest, is the curved tape. With 'C' or 'S' cross sections, stiffness is achieved in the same way as a hardware store variety tape measure. The 'S' section has the advantage of preventing machining or thermal stress biases which might be caused by the asymmetrical 'C' section. These biases lead to a curvature to the boom even when it is unloaded. Although any of these devices would provide sufficient stiffness for the tail boom, the tubes require larger deployment devices. The 'S' section curved tape is the most promising option at this time. A motor may be used to deploy the boom, but it is possible to design these devices to extend under their own spring force.

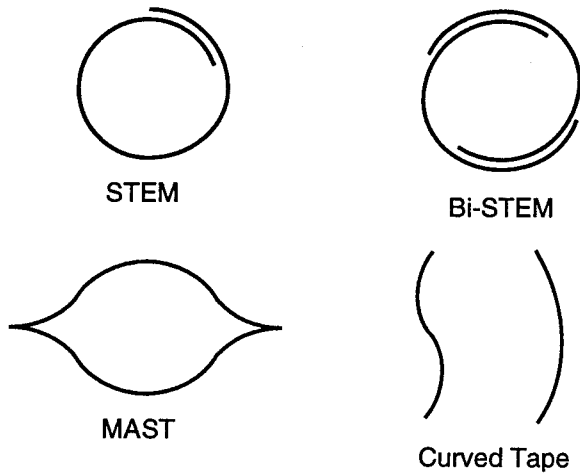


Figure IX.2: Sample Cross Sections of Deployable Booms

To deploy the end plate, a single deployable tape would be fastened to the plate and to the spacecraft. The tape could be wound around a drum or the spacecraft bus itself. The plate would consist of a membrane of film or foil supported by a rigid structure. The tape would attach to the center of the plate structure to minimize aerodynamic shadowing. The wiring would pass

along the tape, and be wound together with the deployable member. These tapes are not the only available deployment option, but demonstrate an effective deployment approach. An actuated truss or inflatable member would likely satisfy the deployment needs of this spacecraft.

For the solar arrays, a spring-hinge and damper will be used. These devices are used in many spacecraft for similar purposes, and an investigation of the available technology was not performed. An actuated latch or pyrotechnic device will be needed to restrain the panel until it is deployed. A metal wire which can be burned like a fuse is also a possibility. Once released, the spring forces the hinge open until it reaches the deployed position. It is either latched in the deployed configuration, or the spring is designed to supply sufficient force to keep the hinge from closing. It will be necessary to wait for the craft to reach a stable attitude before deploying the solar array to ensure that the Earthward panel remains closed.

The 2 m long vertical (z direction) member could be constructed as a deployable mechanism, but it may not be advantageous. The stowed dimension is limited to the diameter of the plate (0.68 m) and the height of the folded solar panels (2 at 0.45 m each). Only 0.4 meters can be gained by using a deployable central member. With the payload electronics split evenly between the two halves, nearly all power and data wires must run along this member. To minimize noise this will likely require shielded cable between the payload boxes. It may be difficult to implement a deployment system that would minimize the thickness of this member and support the wires. Allowing the central member to remain a non-actuated unit, may prove more effective because of the electrical components.

X Overall Feasibility & Conclusions

Now that the individual subsystems have been analyzed, and possible design approaches explored; the overall concept feasibility is examined. Feasibility, for the purposes of this report, refers to the capability of creating a satellite using available technology that will be able to return useful science data. The usefulness of the data is determined by comparing it to the currently available data set and seeing if an improvement is made. The analyses to this point have shown that it is possible to construct a spacecraft that will return science data that is at least as good as that which has been obtained to date. However, to do so, a mechanical damping device capable of sufficient energy dissipation at very low rates must be located or designed. In addition, the noise in the differential GPS phase measurement must be reduced to 1 mm of phase. If these capabilities, can be met, then the spacecraft concept is feasible.

The phase measurement capability of available GPS receivers is not well known. This experiment would represent a case which is not typical of the applications to date. In conventional applications the uncertainty in the phase measurement is primarily due to multipath effects. The multipath conditions for this satellite will be minimized through geometric analysis and careful design. It is unlikely that a high level of confidence can be achieved without experimentation, or simulation of the multipath environment caused by spacecraft self-viewing. It is imperative, however, that great care be taken to quantify this multipath environment.

The mechanical damping concerns remain the greatest unknown in the spacecraft design. It may be possible to construct a rotary damping device at the tail support that would give responses similar to the one in Figure VII.11. However, the average

measurement error for this case is larger than 10 m/s which is not competitive with other techniques. It is possible that better responses can be had by varying the properties of the rotary joint, but additional simulation would be required. Active damping is also a possibility, and sufficient attitude measurements are made to estimate the spacecraft yaw rates. The use of an active control system may defeat the attempt to create a simple measuring system.

In short, the theory supports the possibility of such a spacecraft (see also Appendix A: Spacecraft Summary). Power and thermal needs are not beyond conventional technology. Gravity gradient stabilization allows the yawing motion to be uncoupled from roll and pitch. A tail plate can be used on a relatively short boom to provide sufficient satellite tracking. Average attitude errors less than 0.5 mradians have been obtained with dynamic simulations in a realistic wind profile. GPS phase measurements in the absence of significant multipath are capable of sufficient resolution to detect the attitude within 0.7 mradians. This would lead to zonal wind measurements within 5 m/s for the lifetime of the spacecraft. All of these would be made possible by a sufficient damping mechanism. In this configuration, the mechanism needs to provide a damping ratio of 0.2.

The lifetime in this case is limited to approximately 3 months. This is enough time to sample a single season. In a polar orbit, nodal regression does not occur so only 12 solar hours would be measured in 3 months due to the revolution of the Earth about the sun. If the inclination were changed from 90° to 83° , sufficient regression would allow the entire solar day to be covered. This would of course prevent readings above 83° latitude where the motion may be the most interesting scientifically. Regardless of inclination; altitude, solar hour, and season will be directly coupled throughout the satellite life. This

causes local solar time and seasonal effects to be indistinguishable. Multiple satellites in different orbits would lead to a better global data set.

The recommendation of this paper is that further analysis should be made on novel damping methods and estimating multipath environment for this spacecraft. Viscoelastic materials may allow a viable damping method. It is also possible that a rotary spring and damper set may be designed to operate at these low rates through mechanical magnification or some other means. In addition to damping devices, experimentation or simulation should be performed to better characterize the multipath environment of the spacecraft. If multipath can be minimized or shown to be negligible as a source of measurement error, conventional GPS receivers will be capable of sufficient angular resolution. With this knowledge, it will be possible to create a satellite with a 3 month lifetime that will provide wind measurement data with accuracies as low as 5 m/s. With the additional location reference provided by the GPS system, a significant improvement over current available data is possible.

XI. References

1. Burrage, M. D., W. R. Skinner, D. A. Gell, P. B. Hays, A. R. Marshall, D. A. Orland, A. H. Manson, S. J. Franke, D. C. Fritts, P. Hoffman, C. McLandress, R. Niciejewski, F. J. Schmidlin, G. G. Shepherd, W. Singer, T. Tsuda, and R. A. Vincent, "Validation of Mesosphere and Lower Thermosphere Winds from the High Resolution Doppler Imager on UARS," *Journal of Geophysical Research*, Vol. 101 (D6), 1996, pp. 10365-10392.
2. Larson, W. J., and J. R. Wertz, *Space Mission Analysis and Design*, Second Edition, Kluwer Academic Publishers, Norwell, MA, 1992.
3. *U.S. Standard Atmosphere, 1976*, NOAA, NASA, U.S. Air Force, Washington, DC, 1976.
4. Moe, K. and M. M. Moe, "Progress in Calculating Satellite Drag Coefficients from orbital Measurements," *19th AIAA Advanced Measurement and Ground Testing Conference*, AIAA 96-2233, New Orleans, 1996.
5. Hays, P. B., V. J. Abreu, M. E. Dobbs, D. A. Gell, H. J. Grassl, and W. R. Skinner, "The High-Resolution Doppler Imager on the Upper Atmosphere Research Satellite," *Journal of Geophysical Research*, Vol. 98 (D6), 1993, pp. 10713-10723.

6. Shepherd, G. G., G. Thuillier, W. A. Gault, B. H. Solheim, C. Hersom, J. M. Alunni, J.-F. Brun, S. Brune, P. Charlot, L. L. Cogger, D.-L. Desaulniers, W. F. J. Evans, R. L. Gattinger, F. Girod, D. Harvie, R. H. Hum, D. J. W. Kendall, E. J. Llewellyn, R. P. Lowe, J. Ohrt, F. Pasternak, O. Peillet, I. Powell, Y. Rochon, W. E. Ward, R. H. Wiens, J. Wimperis, "WINDII, the Wind Imaging Interferometer on the Upper Atmosphere Research Satellite," *Journal of Geophysical Research*, Vol. 98 (D6), 1993, pp. 10725-10750.
7. Fleming, E. L., S. Chandra, M. D. Burrage, W. R. Skinner, P. B. Hays, B. H. Solheim, and G. G. Shepherd, "Climatological Mean Wind Observations from the UARS High-Resolution Doppler Imager and Wind Imaging Interferometer: Comparison With Current Reference Models," *Journal of Geophysical Research*, Vol. 101 (D6), 1996, pp. 10455-10473.
8. Moran, Barbara, "Back to Basics," *New Scientist*, Vol. 151, 1996.
9. Cohen, C. E., "Attitude Determination," *Global Positioning System: Theory and Applications*, Vol. II, 1996, pp. 519-538.
10. GANE Home Page: <http://sspp.gsfc.nasa.gov/gane.html>, March 17, 1996.
11. Osborne, M. L., and R. H. Tolson, "GPS Attitude Determination Using Deployable-Mounted Antennas," NASA CR 4721, Langley Research Center, March 1996.
12. Ulrich, P., Mucklow, G., NASA OSS Advanced Technology and Mission Studies: www.hq.nasa.gov/office/oss/osstech/tech_techno.html, February 7, 1997.

13. Chemlelewski, A. B., "Lithium Battery for Space Exploration," *Proceedings of the 30th Intersociety Energy Conversion Engineering Conference*, Orlando, 1995.
14. Sewell, K., "New Military Battery Technologies Trade Chemicals For Plastic," *Military & Aerospace Electronics*, December 1996, p. 21.
15. Nickel Cadmium Cells For Space Application, SAFT Advanced Battery Group, Romainville, France, Sales Document, Ref. DES/EDS/1014/89.
16. Kaplan, M. H., *Modern Spacecraft Dynamics and Control*, John Wiley & Sons, Inc., New York, 1976, pp. 199-204.
17. Meirovitch, L., *Methods of Analytical Dynamics*, Reissue, McGraw-Hill, Inc., New York, 1988, pp. 470-475.
18. Hedin, A. E., Spencer, N. W., Killeen, T. L., "Empirical Global Model of Upper Thermosphere Winds Based on Atmosphere and Dynamics Explorer Satellite Data," *Journal of Geophysical Research*, Vol. 93 (A9), pp. 9959-9978.
19. Constantinescu, V. N., *Laminar Viscous Flow*, Springer-Verlag New York, Inc., New York, 1995, pp. 189-195.
20. Boyle, W. P., *Applied Fluid Mechanics*, McGraw-Hill Ryerson Limited, Toronto 1986, p. 329.
21. Lenhoff, J., Private conversation regarding Colorless Oxygen Resistant film, Triton Systems, Inc., January 13, 1997.

22. Beer, F. P., and Johnston, E. R. Jr., *Mechanics of Materials*, Second Edition, McGraw-Hill, Inc., New York, 1992.
23. Crawford, R. F., "Strength and Efficiency of Deployable Booms for Space Applications," *AAS/AIAA Variable Geometry and Expandable Structures Conference*, AIAA No. 71-396, American Institute of Aeronautics and Astronautics, 1971.
24. Rennie, B. B., "New Closed Tubular Extendible Boom," *Proceedings of the 2nd Aerospace Mechanisms Symposium*, NASA TM 33-355, Jet Propulsion Laboratory, 1967, pp. 163-169.

Appendix A: Spacecraft Summary

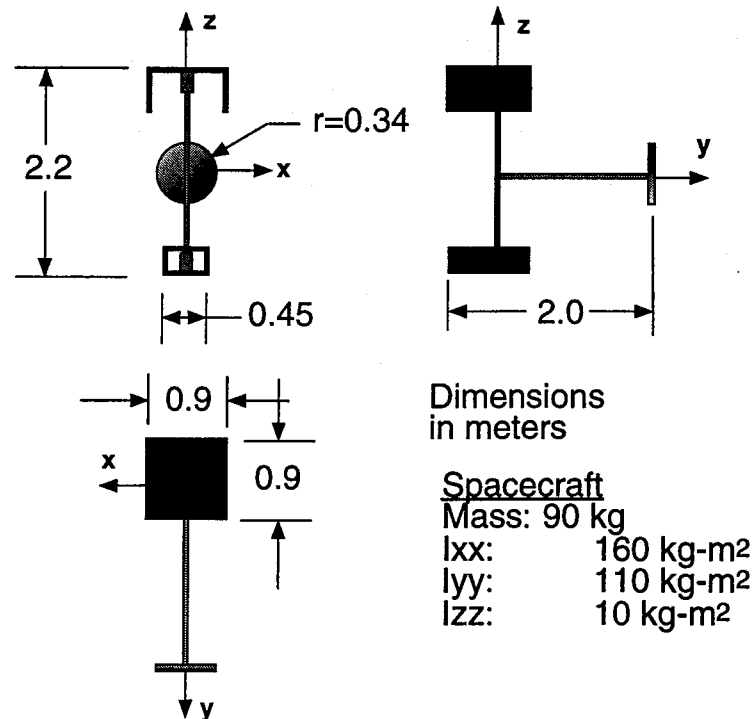


Figure A.1: Spacecraft Dimensions and Summary

Maximum Stowed Dimensions	_____	0.7 x 0.9 x 2.2 m
Maximum Deployed Dimensions	_____	0.9 x 2.0 x 2.2 m
GPS Phase Resolution	_____	1 mm
Wind Velocity Resolution	_____	7 m/s
Peak Solar Power	_____	110 W at 28V
Solar Panel Efficiency	_____	10%
Maximum Energy Use per Orbit	_____	33.4 W-hrs
Minimum Solar Energy per Orbit	_____	40 W-hrs
Battery Capacity	_____	1.5 A-hrs
Battery Package Dimensions	_____	6 x 8 x 12 cm
Equilibrium Temperature Range	_____	275-300°K
Target Damping Coefficient (ζ)	_____	0.20
Uplink Margin for 2.3 GHz	_____	19 dB
Downlink Margin for 2.5 GHz	_____	12 dB
Payload Box Dimensions (2)	_____	6 x 13 x 75 cm